IEEE Access
Multidisciplinary | Rapid Review | Open Access Journal

Received 14 March 2023, accepted 30 March 2023, date of publication 5 April 2023, date of current version 11 April 2023.

Digital Object Identifier 10.1109/ACCESS.2023.3264833

RESEARCH ARTICLE

Adaptive Robust Unit Commitment of Combined-Cycle Gas-Turbine Considering Mode-Based Modeling of Carbon Capture Plant

LUYU WANG[1], (Graduate Student Member, IEEE), BOYOU JIANG[1], YUNHUI SHI[2], AND ZHE CHEN[3]

[1]School of Electrical Engineering, Zhejiang University, Hangzhou 310027, China
[2]Power Dispatch and Control Center, State Grid Zhejiang Electric Power Company Ltd., Hangzhou 310007, China
[3]Electric Power Research Institute, State Grid Zhejiang Electric Power Company Ltd., Hangzhou 310014, China

Corresponding author: Luyu Wang (wang_luyu@zju.edu.cn)

This work was supported by the National Natural Science Foundation of China under Grant U22B2098.

ABSTRACT The power sector bears significant responsibility for achieving carbon neutrality. Low-carbon, high-flexibility generation technologies are pivotal in the generation mix of the foreseeable future. In this paper, a mixed-integer operation model of combined-cycle gas-turbine generators is developed, featuring a new mode-based modeling of post-combustion carbon capture plants. The model is applied to a day-ahead adaptive robust unit commitment problem considering wind power uncertainties. Numerical results from a case study on a modified 39-bus benchmark system demonstrate the correctness and practicality of the model. Compared to the linear model widely adopted in the literature, the proposed mode-based model achieves a 4.91% wider operating range in the net electric power output. Besides, the initial solvent ratio is identified as a non-negligible parameter for the short-term operation of carbon capture plants, whose optimal setting leads to a wider operating range in the net electric power output of up to 21.96%.

INDEX TERMS Adaptive robust optimization, carbon capture plant, CCUS, unit commitment.

NOMENCLATURE

Acronyms:

ARO	Adapative robust optimization
C&CG	Column & constraint generation
CCGT	Combined-cycle gas turbine
CCP	Carbon capture plant
CCSP	Chance-constrained stochastic programming
DRO	Distributionally robust optimization
ED	Economic dispatch
MR	Maximum regeneration
PTDF	Power transfer distribution factor
RO	Robust optimization
RPL	Regular part-load
SP	Stochastic programming
SS	Solvent storage
UC	Unit commitment

Parameters:

$\acute{R}$	generator maximum ramp-up power (MW/hour)
ΔW^{dn}	wind power forecast error lower bound (MW)
ΔW^{up}	wind power forecast error upper bound (MW)
$\grave{R}$	generator maximum ramp-down power (MW/hour)
$\overline{f}$	power transmission line capacity (MW)
$\overline{m}$	solvent storage tank capacity (10^3 kg)
$\overline{P}$	generator maximum output power (MW)
$\underline{P}$	generator minimum output power (MW)
$\widehat{W}$	wind power scenario (MW)

The associate editor coordinating the review of this manuscript and approving it for publication was Ragab A. El-Sehiemy.

a_0^{mr} constant term in the net power output deviation model of the CCGT-CCP under MR mode (MW)
a_0^{rpl} constant term in the net power output model of the CCGT-CCP under RPL mode (MW)
$a_0^{\mathrm{sol,mr}}$ constant term in the inbound solvent flow model of the CCP under MR mode (10^3 kg)
$a_0^{\mathrm{sol,ss}}$ constant term in the outbound solvent flow model of the CCP under SS mode (10^3 kg)
a_0^{ss} constant term in the net power output deviation model of the CCGT-CCP under SS mode (MW)
a_1^{mr} coefficient in the net power output deviation model of the CCGT-CCP under MR mode (MW/percentage)
a_1^{rpl} coefficient in the net power output model of the CCGT-CCP under RPL mode (MW/percentage)
$a_1^{\mathrm{sol,mr}}$ coefficient in the inbound solvent flow model of the CCP under MR mode (10^3 kg/percentage)
$a_1^{\mathrm{sol,ss}}$ coefficient in the outbound solvent flow model of the CCP under SS mode (10^3 kg/percentage)
a_1^{ss} coefficient in the net power output deviation model of the CCGT-CCP under SS mode (MW/percentage)
B^{d} weighted sum of PTDF of bus loads
B^{w} weighted sum of PTDF of wind farms
c^{fuel} generator operation variable cost ($ 100/MW)
c^{ls} load shedding penalty cost ($ 100/MW)
c^{on} generator operation fixed cost ($ 100)
c^{su} generator start-up cost ($ 100/MW)
c^{wc} wind curtailment penalty cost ($ 100/MW)
D system load forecast (MW)
h^{gen} PTDF of generators
M the uncertainty budget
m_0 initial solvent mass in the storage tank (10^3 kg)
V^{off} generator minimum off periods
V^{on} generator minimum on periods
W wind power forecast (MW)

Sets:

$\mathcal{G}$ the index set of dispatchable generators
$\mathcal{G}^{\mathrm{CCP}}$ the index set of CCGT-CCPs
$\mathcal{G}^{\mathrm{coal}}$ the index set of coal-fired generators
$\mathcal{G}^{\mathrm{GT}}$ the index set of GT generators
$\mathcal{L}$ the index set of transmission lines
$\mathcal{T}$ the index set of dispatch periods
$\mathcal{U}$ the uncertainty set

Decision Variables:

$\boldsymbol{p}^{\mathrm{e}}$ electric power outputs; continuous
$\boldsymbol{p}^{\mathrm{ls}}$ shedded load power; continuous
$\boldsymbol{p}^{\mathrm{wc}}$ curtailed wind power; continuous
$\boldsymbol{s}$ auxiliary variables for start-up indicator
$\boldsymbol{u}^{\mathrm{dn}}$ wind forecast error lower bound indicator
$\boldsymbol{u}^{\mathrm{up}}$ wind forecast error upper bound indicator
$\boldsymbol{v}$ commitment state indicator
$\boldsymbol{x}$ output level of CCGT in percentage; continuous
$\boldsymbol{y}$ SS mode indicator
$\boldsymbol{z}$ MR mode indicator
Θ the value function of the recourse problem

I. INTRODUCTION

The latest IPCC assessment report predicts that global warming of $1.5°C$ would likely be exceeded in the near term (before 2040) if a very high greenhouse gas emission remains the status quo [1]. Coaction among key sectors such as energy, industry, transport, and agriculture is decisive to climate change mitigation and adaptation. Deep decarbonization of the power sector bears significant responsibility for achieving carbon neutrality. Extremely high or even 100% renewable energy power systems is one solution to decarbonization [2]. However, the feasibility of such systems correlates primarily to the abundance and geographical distribution of natural resources [3]. For instance, a recent comprehensive review of the development of renewable energy sources in Egypt indicates that the current integration level has already challenged the power grid [4]. Therefore, utilizing a diversity of low-carbon generation technologies, such as biomass power generation or fossil fuel generation plants with carbon captures, could be more attractive from an economic perspective [5]. A bibliometric analysis of recent reports on carbon capture and storage project investment and planning can be found in [6].

In research on the operation of bulk power systems, generators with carbon capture plants (CCPs) have drawn increasing attention. Reference [7] considered CCPs in a single-period robust environmental economic dispatch (ED) problem, addressing a trade-off between the power system's operation cost and carbon emission. In [8], [9], and [10], multi-period ED problems were studied, considering CCPs as contributors to system flexibility and other flexibility sources such as demand response and battery-based energy storage systems. Uncertainties about renewable energy were tackled with stochastic programming and robust interval optimization. Besides, [10] reported results under a carbon-trading market setting where the power system is operated in a distributed manner. Given that natural gas is a cleaner primary energy source compared to coal, [11] and [12] considered CCPs in electricity-gas co-optimization problems. Reference [11] demonstrated the benefits of a carbon-cycle nexus which consists of fossil-fuel generators with CCPs and power-to-gas equipment, especially its contribution to decreasing wind power curtailment. Reference [12] proposed a chanced-constrained stochastic programming model to balance the risk of system power mismatch and the costs from CCPs and demand response.

Studies on the operation of integrated energy systems give rising prominence to CCPs as well. In [13], [14], [15], [16], and [17], the carbon-cycle nexus was integrated into multi-period ED problems. The nexus includes new

technologies such as supercritical carbon-cycle systems and waste incineration. For uncertainties, chance-constrained stochastic programming and data-driven robust optimization are used. For moderately large-scale systems, electricity-gas co-optimization problems are also interesting. In [18], a multi-period unit commitment (UC) model was proposed to quantify the potential synergy of CCPs, demand response, and electric vehicles. Fuzzy chance-constrained stochastic programming was adopted to treat uncertainties.

The operational models of CCPs in the above-motioned literature were uniformly based on or simplifications of the work of Chen and co-authors as in [19]. However, different models of CCPs highlighting several interesting aspects of operation problems were proposed in a handful of papers. [20] offered a multi-layer decision support framework, aiming at year-long revenue maximization of the generation enterprise. The bottom-level dynamic model of the CCPs was navigated by the middle-level model-predictive control scheme, which was further embedded into the top-level economic optimization model. Price signals of both electricity and carbon trading were directly fed into the top level. Neither other Gen-Cos nor the transmission system was considered. In [21], neural networks were used to fit the static model of CCPs. The multi-input multi-output model maps internal variables to external variables of the operation of the CCPs, resulting in a black-box correlation model. Albeit giving a panoramic view of the operational details, the model was set to support equipment installation and phase-out decisions. The scheduling problem was considered in a succinct form. In [22], the modeling methodology was similar to that in [19], though the emphasis was monetary. It's noteworthy that the model also took into account variations in coal quality. Unit commitment without transmission constraints was used as the base problem.

A systemic characterization of the related pieces of literature is summarized in Table 1. Surprisingly, [19] stands out as the predominant source of the modeling of CCPs in power system operations research. 13 out of 16 papers adopted the original or a simplified model as in [19]. As will be shown in Section II, the model in [19] is coarse yet basically correct, let alone the absence of empirical evidence supporting the model's correctness. Additionally, solvent storage in CCPs is ignored in most papers. Integrating solvent storages in CCPs will greatly widen the operating range of the net power output, which benefits power systems' flexibility from the generation side. Finally, uncertainties about renewable energies will only be more prominent in deep decarbonization. Proper treatment of uncertainties in power system operation problems is necessary.

This work aims to contribute to the above discourse, focusing on the operational modeling of CCPs for short-term operation scheduling of power systems under uncertainties. Specifically,

- A new mode-based model of CCPs is proposed. The modeling builds upon new empirical evidence in [23] on the optimal operation of CCPs. The model follows a new set of operation modes of CCPs. The net power outputs of the combined-cycle gas turbine (CCGT) under each operation mode of CCPs are described by mixed-integer affine expressions.
- An adaptive robust day-ahead UC model is developed considering the mixed-integer CCGT-CCP model. Uncertainties from wind powers are modeled using the box set with cardinal constraint (uncertainty budget). The problem is solved by the duality-based column & constraints generation decomposition method.
- The storage tank's initial solvent ratio is identified as a meaningful operation parameter in short-term power system operation problems. Justification is based on numerical results from a case study.

The rest of this paper is outlined as follows. Section II presents the proposed mode-based model of CCPs and the mixed-integer operational model of the CCGT-CCPs. Section III briefs the mathematical formulation of the adaptive robust UC problem and the column & constraint generation decomposition method. The configuration of the case study is given in Section IV. Numerical results and discussion are delivered in Section V. Section VI concludes the paper and directs to future works.

II. A MIXED-INTEGER OPERATIONAL MODEL OF THE CCGT-CCP

This Section introduces the proposed mixed-integer operational model of the CCGT-CCP after a quick examination of the workflow of the CCP and a concise survey of the line of work on the operational modeling of CCPs for power system operation problems.

A. THE OPERATION WORKFLOW OF CCPs

Figure 1 depicts a typical carbon capture plant with solvent storage. Flue gas from the main boiler is first fed into the bottom of the absorber. It will confront the showering-down lean solvent along the way up. A large percentage of the CO_2 in the flue gas will be absorbed into the lean solvent during the process. The lean solvent becomes 'rich' after being loaded with CO_2 and will be pumped into the stripper. The rich solvent unloads the captured CO_2 in the stripper. The unleashed CO_2 expands to the top while the regenerated lean solvent falls to the bottom. The lean solvent will then be recirculated back to the top of the absorber to continue the loop.

It is self-evident that the circulation of the solvent should keep up with the flow rate of the flue gas if a fixed percentage of carbon capture (usually called the *capture rate*) is targeted. Consequently, the flow rate of the lean solvent and the rich solvent are bonded. As the stripper, more precisely the reboiler, is heated by the medium-/low-pressure steam extracted from the main boiler, the electricity generation suffers from a fixed loss (usually called the *energy penalty*). Such inflexibility is undesirable in the evolving generation mix comprising excessive intermittent and fluctuant energy

TABLE 1. Systematic characterization of related literature.

Reference	CCP model	Solvent tank considered?	Target system type	Scheduling problem model	Power flow considered?	Uncertainty framework
[7]	Chen's	No	bulk grid	s-ED	Yes	RO
[8]	Chen's	Yes	bulk grid	m-ED	Yes	SP
[9]	Chen's	Yes	bulk grid	m-ED	Yes	ARO
[10]	Chen's	Yes	bulk grid	m-ED	Yes	N/A
[11]	Chen's	No	bulk grid	m-UC	Yes	N/A
[12]	Chen's	No	bulk grid	m-UC	Yes	SP
[21]	Neural Network	No	bulk grid	m-ED	No	N/A
[22]	Monetary	No	bulk grid	m-UC	No	N/A
[13]	Chen's	No	IES	m-ED	No	N/A
[14]	Simple	No	IES	m-ED	No	N/A
[15]	Chen's	No	VPP	m-ED	No	CCSP
[16]	Simple	No	IES	m-ED	No	RO
[17]	Simple	N0	IES	m-ED	No	DRO
[18]	Simple	No	IES	m-UC	Yes	fuzzy CCSP
[20]	Dynamic	No	Plant	m-UC	Yes	N/A

Notes: *s-*: single-period; *m-*: multi-period; *ED*: economic dispatch; *UC*: unit commitment; *RO*: robust optimization; *SP*: stochastic programming; *ARO*: adaptive robust optimization; *CCSP*: chance-constrained stochastic programming; *DRO*: distributionally robust optimization;

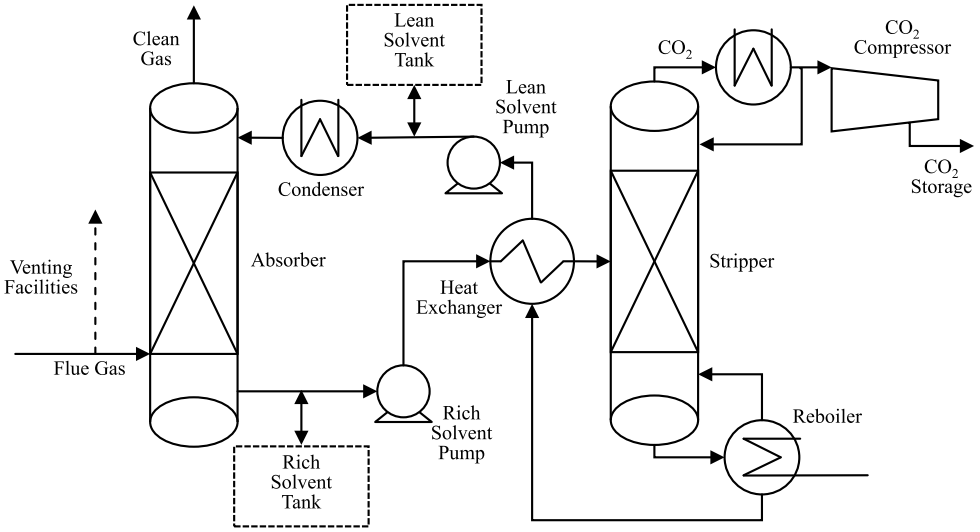

FIGURE 1. Operation workflow of a typical carbon capture plant with solvent storages [24].

sources such as wind and solar power. Enhancing CCPs' flexibility holds both technical and economic value.

B. COMMENTS ON KEY REFERENCES

To the best of the authors' knowledge, the concept of flexible operation of the CCPs was first proposed in [25] by Lucquiaud and colleagues. CCP with solvent storage was shown to be beneficial to the flexibility of the host generation plant. The paper documented a key observation that with solvent storage, solvent regeneration could be temporally decoupled from the host plant's main boiler, which is the heat source of both electricity generation and carbon capture. The decoupling enables the operator to adjust the intensity of solvent regeneration, hence the net electric power output of the generator, in response to electricity price signals. The modeling counted detailed thermo-dynamics. However, the overall focus of the work is on plant-wise operation.

In [19], Chen and co-authors introduced the operation of CCPs to the power systems operation research community. Post-combustion capture plants with aqueous solvent storage were regarded as the most mature technology. A mathematical model of the operations of CCPs was established by employing a set of external variables. Internal workings were masked by the efficiency parameter. Despite its suitability for power systems operation problems, the model fails to appreciate the flexibility of the reboiler. It attributes altered energy penalties entirely to variants in the quantity of flue gas that needs to be processed, either due to a changed output level of the main boiler or the percentage of flue gas that the CCP bypasses. Besides, the model was developed assuming all internal mechanisms of CCPs are roughly

linear, yet no validating evidence was provided to support the premise.

In [26], Martens and co-authors proposed a mixed-integer model of CCPs for UC problems. The model distinguished the 'off' state and the 'standby' state of CCPs. The former refers to a complete halt of the whole system, with no heat consumption from the main boiler. The latter refers to a minimum heat consumption that is just enough to keep the CCP on but impossible to perform carbon capture. The model also accounted for the start-up state of CCPs. It acts as a necessary transition from the 'off' state to the 'standby' or the 'on' state. It may also better estimate the carbon emission during the state transition. Although the model is intuitive and resembles the UC model of generators, its rationality bears the burden of proof. Note that a typical dispatch period in UC is 1 hour. It is questionable why the cold reboiler would need such a long time to heat up, given its designed thermal capacity is only a fraction of the main boiler. As every state asks for its corresponding binary variable whose quantity has a considerable influence on the performance and scalability of the model, the necessity of the off state begs further examination.

What is also worth mentioning is that all the host generation plants considered in the works mentioned above are coal-fired thermal plants. CCGTs might be more favorable over coal-fired thermal plants from several aspects, such as efficiency, flexibility, and carbon emission intensity. The relevance of CCGTs in future generation mix potentially overshadows that of coal-fire thermal plants.

In contrast, the work of Spitz and co-authors in [23] distinguishes itself from [19], [25], and [26] in the following three aspects:

- The study was conducted using state-of-the-art commercial simulation software. The power cycle and the carbon capture process are modeled in gPROMS, and the gas-turbine model is provided by Thermoflow GT Master. Both models are dynamic.
- The adopted control strategy on the CCP was clarified. The reasoning behind the adoption was also documented based on a comparison of common control strategies in the literature and a clear statement of the authors' design intent.
- Internal operation variables such as stripper pressure were optimized to achieve the lowest energy penalty. The resulting characterization of external operation variables can be directly used by steady-state models such as day-ahead UC and ED problems.

Accordingly, the results in [23] lay an updated and more solid foundation for modeling CCPs in power system operation research.

C. THE PROPOSED MODE-BASED MODEL OF CCPs

The following mode-based model of the CCPs is proposed regarding the spotted gaps. It extrapolates the results in [23], giving a generic description of the operation of CCPs. The operation is conceptualized to consist of 4 distinct modes:

1) The bypass mode
   The bypass mode refers to the 'off' state of the CCP. Contrary to [26], the 'off' state and the 'standby' state of the CCP are lumped together. Under the bypass mode, the flue gas emitted from the main boiler is not processed and is entirely vented into the atmosphere. From the power system operators' standpoint, the mathematical model of the whole plant falls back to the host generation plant.
2) The regular part-load (RPL) mode
   The regular part-load mode of the CCP accompanies the part-load operation of the host generation plant. Under this mode, the CCP is controlled to keep a constant capture rate. A fixed proportion of CO_2 is captured anywhere in the operation range of the base plant. The lean solvent is withdrawn to wash the flue gas, while the rich solvent is boiled to regenerate the lean solvent. The solvent cycle enters a balance: net changes in either the rich or lean solvent tank are equal to zero. The energy penalty is minimized.
3) The maximum regeneration (MR) mode
   The maximum regeneration mode results from shifting the regular part-load mode toward maximum lean solvent regeneration. Under this mode, the CCP regenerates as much of the rich solvent as the boiler's capacity allows. The rich solvent tank depletes at the maximum rate. The energy penalty increases as an extra amount of rich solvent is regenerated, and the stripper derails from its most energy-efficient configuration.
4) The solvent storage (SS) mode
   The solvent storage mode is the opposite of the maximum regeneration mode. It shuts down the regeneration completely. Under this mode, the minimum energy penalty is achieved, as only the solvent circulation and the compression of the captured CO_2 requires power supplies. Storage tanks become the only source and the only sink of the solvent. If the rich or lean solvent tank is depleted, the CCP will be forced back to the regular part-load mode.

Note that the bypass mode is omitted in the following operation model of CCGT-CCP. Three observations could justify the omission. First, bypassing decisions could only be objectively evaluated where carbon emission is appropriately priced. Examples are carbon markets or carbon taxation schemes. As such a context is beyond the scope of this paper, including the bypass mode is unnecessary. Second, bypassing is less likely to be allowed in the future, where more stringent decarbonization regulation could be expected. Last, covering the bypass mode shares the same technique as the other modes. Introducing a new set of binary variables will do. Consequently, omitting the bypass mode is preferable.

D. A MIXED-INTEGER OPERATION MODEL OF CCGT-CCP

The mode-based model of CCPs naturally calls for a mixed-integer model of the net power output model. Binary variables indicate the engagement of the modes. The power

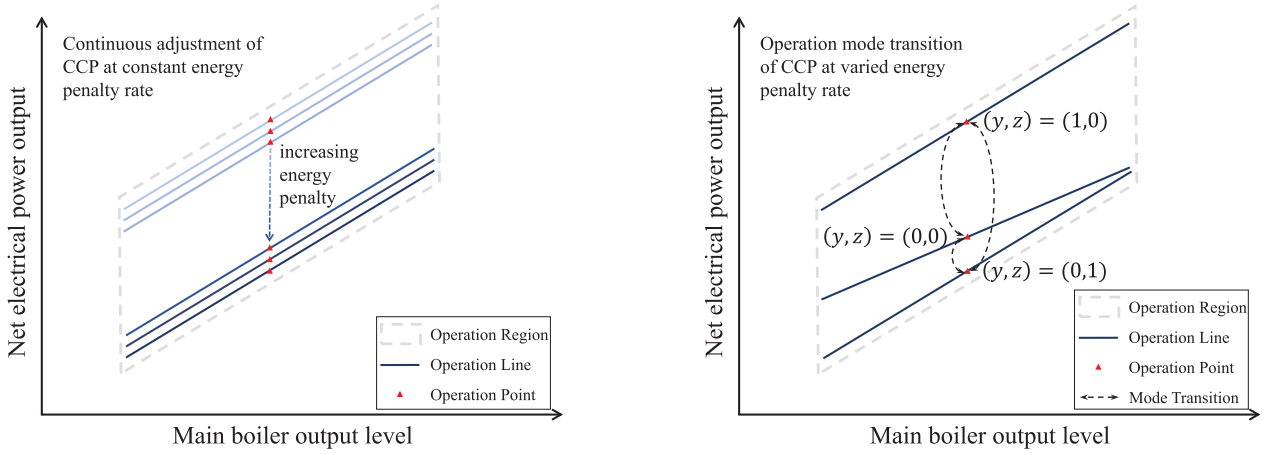

(a) Chen's linear model

(b) The proposed mode-based model

FIGURE 2. Geometric implication of Chen's linear model and the proposed mode-based model.

outputs are described as affine functions of the main boiler load level. The RPL mode is treated as the base mode. Net power outputs under the SS and MR modes are viewed as deviations from the base mode. The net power output of the CCGT-CCP under the RPL mode is given by (1)

$$P_t^{\mathrm{e,rpl}} = a_1^{\mathrm{rpl}} x_t + a_0^{\mathrm{rpl}} v_t, \quad \forall t \in \mathcal{T}, \tag{1}$$

where $P_t^{\mathrm{e,rpl}}$ stands for the electric power output of the whole plant under the regular part-load mode in period t, a_1^{rpl} and a_0^{rpl} are coefficients of the first-order and the constant terms, x_t is the load level (in percentage) of the base gas turbines, v_t is the binary variable representing the on/off state of the gas turbines.

Deviations of the net power output of the CCGT-CCP under the MR mode and the SS mode are modeled by (2) and (3), respectively:

$$\Delta P_t^{\mathrm{e,ss}} = y_t \left(a_1^{\mathrm{ss}} x_t + a_0^{\mathrm{ss}}\right), \quad \forall t \in \mathcal{T}, \tag{2}$$

$$\Delta P_t^{\mathrm{e,mr}} = z_t \left(a_1^{\mathrm{mr}} x_t + a_0^{\mathrm{mr}}\right), \quad \forall t \in \mathcal{T}, \tag{3}$$

where $\Delta P_t^{\mathrm{e,ss}}$ and $\Delta P_t^{\mathrm{e,mr}}$ are absolute power output deviations under the SS or the MR mode with respect to the RPL mode, y_t and z_t are binary variables indicating whether the CCP is set to work under the corresponding mode, and a_1^{ss}, a_0^{ss}, a_1^{mr}, and a_0^{mr} are all coefficients following a similar convention as in (1).

Let P_t^{e} denotes the electric power output of the CCGT-CCP at dispatch period t. The following equality holds:

$$P_t^{\mathrm{e}} = P_t^{\mathrm{e,rpl}} + \Delta P_t^{\mathrm{e,ss}} - \Delta P_t^{\mathrm{e,mr}}, \quad \forall t \in \mathcal{T}. \tag{4}$$

Note that the deviations of net power output are defined as absolute values. The signs before $\Delta P_t^{\mathrm{e,mr}}$ and $\Delta P_t^{\mathrm{e,ss}}$ in (4) reflect that solvent regeneration draws power from the CCGT, while pure absorption needs little power. Compared to the RPL mode, the net power increases under the MR mode while it decreases under the SS mode.

Apart from affecting the net power output of the CCGT, CCP's operation modes are also coupled with the commitment state of the CCGT:

$$y_t - v_t \le 0, \quad \forall t \in \mathcal{T}, \tag{5}$$

$$z_t - v_t \le 0, \quad \forall t \in \mathcal{T}, \tag{6}$$

$$y_t + z_t \le 1, \quad \forall t \in \mathcal{T}. \tag{7}$$

(5) and (6) indicate that the CCP should be off if the CCGT is off. (7) guarantees that the CCP would only operate under one single mode at any given period.

Another set of constraints on the operation of CCP comes from solvent circulation. As the law of conservation of matter holds, if the solvent is assumed to be lossless, the solvent level in the lean solvent storage tank will always be complementary to that of the rich solvent tank. Examination of just one side of the circulation is enough. Therefore, only the circulation of the lean solvent is considered. Besides, since both sides involve equality constraints, modeling only one side also reduces unnecessary numerical inconsistency due to finite-precession arithmetics.

Notice that the CCP withdraws lean solvent from the storage tank under the SS mode while filling it under the MR mode. The corresponding constraints read as follows:

$$\dot{m}_t^{\mathrm{in}} = z_t \left(a_1^{\mathrm{sol,mr}} x_t + a_0^{\mathrm{sol,mr}}\right), \quad \forall t \in \mathcal{T}, \tag{8}$$

$$\dot{m}_t^{\mathrm{out}} = y_t \left(a_1^{\mathrm{sol,ss}} x_t + a_0^{\mathrm{sol,ss}}\right), \quad \forall t \in \mathcal{T}, \tag{9}$$

$$m_t = m_0 + \sum_{k=1}^{t} \left(\dot{m}_k^{\mathrm{in}} - \dot{m}_k^{\mathrm{out}}\right), \quad \forall t \in \mathcal{T}, \tag{10}$$

$$0 \le m_t \le \overline{m}, \quad \forall t \in \mathcal{T}, \tag{11}$$

where $\dot{m}_t^{\mathrm{in}}$ and $\dot{m}_t^{\mathrm{out}}$ refer to the mass of the solvent that flows into and out of the storage tank in period t; $a_1^{\mathrm{sol,mr}}$, $a_0^{\mathrm{sol,mr}}$, $a_1^{\mathrm{sol,ss}}$, and $a_0^{\mathrm{sol,ss}}$ are all coefficients of the proper unit; m_t is

the mass of solvent contained in the storage tank in period t, and m_0 is the initial value of m_t at the beginning of the dispatch horizon; $\overline{m}$ is the capacity of the solvent storage tanks. (8)-(11) together ensure that the solvent flow matches the operation mode of the CCP and the load level of the base generator, and the solvent in storage will always be in range.

It is sensible to require the solvent mass in the storage to return to its initial value at the end of the day, as this will facilitate the day-to-day scheduling of the CCGT-CCP [27]. The return translates to the net change of the solvent mass in the storage over the whole day equals zero:

$$\sum_{t\in\mathcal{T}}\left(\dot{m}_k^{\text{in}}-\dot{m}_k^{\text{out}}\right)=0. \tag{12}$$

The necessity of (12) depends in part on the time scale of the dispatch horizon. As will be demonstrated in Section V-C, the flexibility of the CCGT-CCP is also affected by (12).

To further expose the differences between the proposed mode-based model and Chen's linear model, the graphs of the net power output in the two models are given in Figure 2. As shown in Figure 2a, the graph of the net power output in Chen's linear model consists of a family of operation lines, each corresponding to a specific energy penalty. The more the CCP processes the captured CO_2, the higher the energy penalty is exerted on the main boiler. The energy penalty rate, the heat demand to process one unit mass of CO_2, is assumed to be constant. So, all the operation lines are in parallel. The operation lines corresponding to higher carbon capture rates that are lower down the vertical axis. The corresponding operation lines form a parallelogram operation region regarding the full range of the processing demand.

In contrast, the proposed mode-based model results from the optimal configuration of the CCP under three typical operation modes, as can be seen in Figure 2b. The energy penalty rate is optimized and varies when the operating point is changed. Flexible operation of the CCP is achieved by mode transitions. The selected operation mode of the CCP and the CCGT load level determine the net electric power output. The mode-based model is an abstraction of the detailed process simulation with optimized parameters, whereas the linear model is deduced from the assumption of a constant energy penalty rate of the CCP. As will be shown in Section V-D, such an assumption leads to an inaccurate estimate of the energy penalty.

III. ADAPTIVE ROBUST UNIT COMMITMENT PROBLEM

This Section presents the generic adaptive robust optimization framework and the detailed formulation of the proposed adaptive robust UC model, followed by the column & constraint generation decomposition algorithm.

A. THE GENERIC ADAPTIVE ROBUST OPTIMIZATION FRAMEWORK

Adaptive robust optimization (ARO), also named adjustable or two-stage robust optimization, addresses sequential decision-making problems under uncertainty. A generic description of ARO problems in compact form can be written as follows [28]:

$$\min_{\boldsymbol{y}}\boldsymbol{c}^\top\boldsymbol{y}+\max_{\boldsymbol{u}\in\mathcal{U}}\min_{\boldsymbol{x}\in\Omega(\boldsymbol{y},\boldsymbol{u})}\boldsymbol{b}^\top\boldsymbol{x} \tag{13}$$

$$\text{s.t. } \boldsymbol{A}\boldsymbol{y}\geq\boldsymbol{d}, \tag{14}$$

$$\boldsymbol{y}\in\mathcal{S}_{\boldsymbol{y}}, \tag{15}$$

$$\Omega(\boldsymbol{y},\boldsymbol{u})=\{\boldsymbol{x}\in\mathcal{S}_{\boldsymbol{x}}:\boldsymbol{G}\boldsymbol{x}\geq\boldsymbol{h}-\boldsymbol{E}\boldsymbol{y}-\boldsymbol{M}\boldsymbol{u}\} \tag{16}$$

where $\boldsymbol{y}$ is the vector of first-stage decision variables, $\boldsymbol{x}$ the second-stage decision variables, and $\boldsymbol{u}$ is the vector of uncertain variables; $\mathcal{S}_{\boldsymbol{y}}$ and $\mathcal{S}_{\boldsymbol{x}}$ refer to the bounds (if available) on $\boldsymbol{y}$ and $\boldsymbol{x}$; $\mathcal{U}$ is the uncertainty set; Ω is the feasible region of the second-stage problem parameterized by the first-stage decision and the uncertainty variables; $\boldsymbol{A}$, $\boldsymbol{G}$, $\boldsymbol{E}$, and $\boldsymbol{M}$ are coefficient matrices; $\boldsymbol{d}$ and $\boldsymbol{h}$ are right-hand-side vectors of proper dimensions. Caution that all symbols in (13)-(16) are chosen arbitrarily for ease of presentation. They do not correspond to the set of symbols in the detailed formulation.

Under the ARO framework, all decision variables are divided into two groups. The *first-stage* variables are supposed to be permanent once decided, while the *second-stage* variables are situational. The second-stage variables are situated by the value of first-stage variables (decisions made) and the uncertain variables (forecast). Mathematically, the second-stage variables are functionals: they are functions of the optimal solution of the first-stage variables and the uncertain variables, which are themselves functions of the problem parameters. The optimization mainly attempts to determine the optimal solution of the first-stage variables, while the second-stage problem essentially serves as a metric. The optimal value of the problem should be interpreted as the objective function's upper bound ascribed to the particular second-stage problem and the uncertainty set. The second-stage problem is often called the *recourse problem*.

The ARO framework matches well with the structure of the UC problem under uncertainty. As commitment decisions are prohibitively expensive to change during real-time operation, even technically impossible for certain generation technologies, they must be decided beforehand. On the other hand, fast-acting generators (e.g., GTs) and some other dispatchable resources (e.g., energy storage) can be re-dispatched when an updated forecast with a higher confidence level is available. The re-dispatch can be modeled as an ED problem or an optimal power flow problem. The objective usually consists of the production cost of the re-dispatched resources and the power imbalance penalties due to either load shedding or wind curtailment.

B. THE PROPOSED ARO UC MODEL

A comprehensive UC model under the ARO framework is first proposed by Bertsimas and co-authors in [29]. In this work, a generation mix consisting of coal-fired plants, GTs, and wind farms is considered. The overall objective of the optimization problem is to minimize the power generation cost and potential power imbalance penalties due to wind

uncertainty. Coal-fired plants usually carry the base load, so both their commitment and power outputs are regarded as first-stage variables. For GTs, the commitment decisions are placed in the first stage, and the power outputs await the second stage. For CCGT-CCPs, the commitment states of the host CCGT and the operation modes of the CCP are decided in the first stage. The power outputs of the CCGT-CCP, and thus the solvent flows, are treated as second-stage decisions. Box uncertainty sets with uncertainty budgets are considered. The box set only requires the upper and the lower bounds on the forecast of the uncertain variables at each dispatch period.

The following fully describes the proposed ARO UC model in its tri-level form. Note that all constraints in the model are presented in the normalized form. Normalization refers to the process of separating constants from expressions of decision variables. After normalization, the left-hand side of each constraint only consists of expressions of decision variables, and the right-hand side only contains constants.

$$\min_{\boldsymbol{v},\boldsymbol{s},\boldsymbol{y},\boldsymbol{z},\boldsymbol{p}^{\mathrm{e}}} \sum_{t\in\mathcal{T}}\Big[\sum_{i\in\mathcal{G}}\left(c_i^{\mathrm{su}}v_{it}-c_i^{\mathrm{su}}s_{it}+c_i^{\mathrm{on}}v_{it}\right) + \sum_{i\in\mathcal{G}^{\mathrm{coal}}} c_i^{\mathrm{fuel}}p_{it}^{\mathrm{e}}\Big] + \max_{\boldsymbol{u}\in\mathcal{U}}\Theta \tag{17}$$

$$\text{s.t. } \forall i\in\mathcal{G},\quad t\in\mathcal{T}:$$

$$v_{it}-v_{i(t-1)}-v_{ih}\le 0,\quad t\le h\le \min\left\{V_i^{\mathrm{on}}+t-1,|\mathcal{T}|\right\}, \tag{18}$$

$$v_{i(t-1)}-v_{it}+v_{ih}\le 1,\quad t\le h\le \min\left\{V_i^{\mathrm{off}}+t-1,|\mathcal{T}|\right\}, \tag{19}$$

$$s_{it}-v_{i(t-1)}\le 0, \tag{20}$$

$$s_{it}-v_{it}\le 0, \tag{21}$$

$$v_{i(t-1)}+v_{it}-s_{it}\le 1, \tag{22}$$

$$v_{it},s_{it}\in\{0,1\}, \tag{23}$$

$$\forall i\in\mathcal{G}^{\mathrm{CCP}},\quad t\in\mathcal{T}:$$

$$\text{constraints (5)-(7)} \tag{24}$$

$$\forall i\in\mathcal{G}^{\mathrm{coal}},\quad t\in\mathcal{T}:$$

$$p_{it}^{\mathrm{e}}-\underline{P}_i v_{it}\ge 0, \tag{25}$$

$$-p_{it}^{\mathrm{e}}+\overline{P}_i v_{it}\ge 0, \tag{26}$$

$$p_{i(t-1)}^{\mathrm{e}}-p_{it}^{\mathrm{e}}+\acute{R}_i v_{i(t-1)}+\underline{P}_i\left(1-v_{i(t-1)}\right)\ge 0, \tag{27}$$

$$p_{it}^{\mathrm{e}}-p_{i(t-1)}^{\mathrm{e}}+\grave{R}_i v_{it}+\underline{P}_i\left(1-v_{it}\right)\ge 0. \tag{28}$$

(17) is the overall objective function, containing the unit commitment cost of all generators, the production cost of all coal-fired generators, and the maximum recourse cost. c_i^{su}, c_i^{on}, and c_i^{fuel} are the coefficients of unit start-up cost, fixed unit operation cost, and marginal production cost, respectively. v_{it} is the on/off state of unit i in dispatch period t. s_{it} is an auxiliary binary variable introduced to exactly model the unit start-up action. p_{it}^{e} is the electric power output of unit i in period t. Θ is the value function of the entire recourse (re-dispatch) problem. $\mathcal{T}$ is the dispatch period index set. $\mathcal{G}$ is the full index set of all generators, with different superscripts indicating the subset of the respective generator type. (18)-(19) limit the minimum on/off periods. (20)-(22) are logical relations that model the exact start-up action. (23) ensures that v_{it} and s_{it} must be binary. For CCGT-CCPs, (24) enforces the operation modes of the CCPs must be unique and dictated by the commitment state. For coal-fired units, (25)-(26) bounds the power output, and (27)-(28) limits the ramping rate between adjacent periods, where $\underline{P}_i$ and $\overline{P}_i$ are the minimum and maximum power outputs, and $\acute{R}_i$ and $\grave{R}_i$ are the maximum ramp-up and ramp-down rates. (17)-(28) constitutes the first-stage problem.

The second-stage problem is a bi-level optimization. The upper level is a maximization problem concerning uncertain variables $\boldsymbol{u}$. A box uncertainty set with cardinality constraints (29)-(31) is used to model how the actualization of the uncertainty would deviate from the forecast.

$$\mathcal{U}=\Big\{u_t^{\mathrm{up}}+u_t^{\mathrm{dn}}\le 1, \tag{29}$$

$$\sum_{t\in\mathcal{T}}u_t^{\mathrm{up}}+u_t^{\mathrm{dn}}\le M, \tag{30}$$

$$u_t^{\mathrm{up}},u_t^{\mathrm{dn}}\in\{0,1\}\Big\}, \tag{31}$$

u_t^{up} and u_t^{dn} are binary variables indicating whether the actualized wind power hits the upper and lower bounds of the forecast error. (29) ensures that the actualized wind power would only deviate in one direction rather than both. (30) is the cardinality constraint, where M is the uncertainty budget. In this work, the uncertainty budget represents the number of dispatch periods where the wind power differs from the forecast value. The larger the uncertainty budget chosen, the higher the variability of the wind power is considered. It is a parameter that reflects the system operators' level of conservativeness.

The lower-level problem, denoted by Θ in (17), is formulated as an optimal power flow problem that aims to minimize both the production cost of the fast-acting units and power imbalance penalties. Note that all first-stage and uncertain variables can be considered constants in the lower-level problem. Expressions introduced by (32)-(33) are devised to ease the normalization of the constraints, where p_{it}^{var} and p_{it}^{fix} are the coefficients and constant terms in the net power output expressions of the CCGT-CCP, and $\dot{m}_{it}^{\mathrm{var}}$ and $\dot{m}_{it}^{\mathrm{fix}}$ are those in the solvent flow expressions. p_{it}^{e} and m_{it} are proxies representing CCGT-CCP's electric power output and the solvent mass in storage. The true decision variables behind the proxies are the CCGT output levels x_{it}.

$$i\in\mathcal{G}^{\mathrm{CCP}},\quad t\in\mathcal{T}:$$

$$\begin{cases} p_{it}^{\mathrm{var}}=a_{1,i}^{\mathrm{rpl}}+a_{1,i}^{\mathrm{ss}}y_{it}-a_{1,i}^{\mathrm{mr}}z_{it},\\ p_{it}^{\mathrm{fix}}=a_{0,i}^{\mathrm{rpl}}v_{it}+a_{0,i}^{\mathrm{ss}}y_{it}-a_{0,i}^{\mathrm{mr}}z_{it},\\ p_{it}^{\mathrm{e}}=p_{it}^{\mathrm{var}}x_{it}+p_{it}^{\mathrm{fix}},\\ \dot{m}_{it}^{\mathrm{var}}=a_{1,i}^{\mathrm{mr,sol}}z_{it}-a_{1,i}^{\mathrm{ss,sol}}y_{it},\\ \dot{m}_{it}^{\mathrm{fix}}=a_{0,i}^{\mathrm{mr,sol}}z_{it}-a_{0,i}^{\mathrm{ss,sol}}y_{it},\\ m_{it}=m_{i0}+\sum_{k=1}^{t}\left(\dot{m}_{it}^{\mathrm{var}}x_{ik}+\dot{m}_{it}^{\mathrm{fix}}\right), \end{cases} \tag{32}$$

The actualized wind power scenario is denoted by $\widehat{W}_t$. It is calculated by (33), where ΔW_t^{up} and ΔW_t^{dn} are forecast errors' upper and lower bounds.

$\forall t \in \mathcal{T}$:

$$\widehat{W}_t = W_t + \Delta W_t^{\mathrm{up}} u_t^{\mathrm{up}} - \Delta W_t^{\mathrm{dn}} u_t^{\mathrm{dn}}, \tag{33}$$

Accordingly, (34)-(50) establishes the lower-level problem.

$$\Theta = \Bigg\{ \min_{\boldsymbol{p}^{\mathrm{e}},\boldsymbol{p}^{\mathrm{wc}},\boldsymbol{p}^{\mathrm{ls}},\boldsymbol{x}} \sum_{t\in\mathcal{T}} \Big[\sum_{i\in\mathcal{G}^{\mathrm{CCP}}} c_i^{\mathrm{fuel}} x_{it} + \sum_{i\in\mathcal{G}^{\mathrm{GT}}} c_i^{\mathrm{fuel}} p_{it}^{\mathrm{e}} + c^{\mathrm{wc}} p_t^{\mathrm{wc}} + c^{\mathrm{ls}} p_t^{\mathrm{ls}} \Big] \tag{34}$$

s.t. $\forall t \in \mathcal{T}$:

$$\sum_{i\in\mathcal{G}^{\mathrm{CCP}}} p_{it}^{\mathrm{var}} x_{it} + \sum_{i\in\mathcal{G}^{\mathrm{GT}}} p_{it}^{\mathrm{e}} - p_t^{\mathrm{wc}} + p_t^{\mathrm{ls}} = D_t - \widehat{W}_t - \sum_{i\in\mathcal{G}^{\mathrm{coal}}} p_{it}^{\mathrm{e}} - \sum_{i\in\mathcal{G}^{\mathrm{CCP}}} p_{it}^{\mathrm{fix}} : \quad (\chi), \tag{35}$$

$\forall i \in \mathcal{G}^{\mathrm{GT}}, \quad t \in \mathcal{T}$:

$$p_{it}^{\mathrm{e}} \geq \underline{P}_i v_{it} : \quad \left(\alpha^{\mathrm{lb}}\right), \tag{36}$$

$$-p_{it}^{\mathrm{e}} \geq -\overline{P}_i v_{it} : \quad \left(\alpha^{\mathrm{ub}}\right), \tag{37}$$

$$p_{i(t-1)}^{\mathrm{e}} - p_{it}^{\mathrm{e}} \geq -\acute{R}_i v_{i(t-1)} - \underline{P}_i \left(1 - v_{i(t-1)}\right) : \quad \left(\beta^{\mathrm{up}}\right), \tag{38}$$

$$p_{it}^{\mathrm{e}} - p_{i(t-1)}^{\mathrm{e}} \geq -\grave{R}_i v_{it} - \underline{P}_i \left(1 - v_{it}\right) : \quad \left(\beta^{\mathrm{dn}}\right), \tag{39}$$

$\forall i \in \mathcal{G}^{\mathrm{CCP}}, \quad t \in \mathcal{T}$:

$$x_{it} \geq \underline{GT}_i v_{it} : \quad \left(\alpha^{\mathrm{lb}}\right), \tag{40}$$

$$-x_{it} \geq -\overline{GT}_i v_{it} : \quad \left(\alpha^{\mathrm{ub}}\right), \tag{41}$$

$$x_{i(t-1)} - x_{it} \geq -\acute{R}_i v_{i(t-1)} - \underline{GT}_i \left(1 - v_{i(t-1)}\right) : \quad \left(\beta^{\mathrm{up}}\right), \tag{42}$$

$$x_{it} - x_{i(t-1)} \geq -\grave{R}_i v_{it} - \underline{GT}_i \left(1 - v_{it}\right) : \quad \left(\beta^{\mathrm{dn}}\right), \tag{43}$$

$$\sum_{k=1}^{t} \dot{m}_{ik}^{\mathrm{var}} x_{ik} \geq -m_{i0} - \sum_{k=1}^{t} \dot{m}_{ik}^{\mathrm{fix}} : \quad \left(\eta^{\mathrm{lb}}\right), \tag{44}$$

$$-\sum_{k=1}^{t} \dot{m}_{ik}^{\mathrm{var}} x_{ik} \geq -\overline{m} + m_{i0} + \sum_{k=1}^{t} \dot{m}_{ik}^{\mathrm{fix}} : \quad \left(\eta^{\mathrm{ub}}\right), \tag{45}$$

$$\sum_{t\in\mathcal{T}} \dot{m}_{it}^{\mathrm{var}} x_{it} = -\sum_{t\in\mathcal{T}} \dot{m}_{it}^{\mathrm{fix}} : \quad (\varphi), \tag{46}$$

$\forall t \in \mathcal{T}$:

$$-p_t^{\mathrm{wc}} \geq -\widehat{W}_t : \quad (\gamma), \tag{47}$$

$$-p_t^{\mathrm{ls}} \geq -D_t : \quad (\iota), \tag{48}$$

$l \in \mathcal{L}, \quad t \in \mathcal{T}$:

$$\sum_{i\in\mathcal{G}^{\mathrm{CCP}}} h_{l,i}^{\mathrm{gen}} p_{i,t}^{\mathrm{var}} x_{i,t} + \sum_{i\in\mathcal{G}^{\mathrm{GT}}} h_{l,i}^{\mathrm{gen}} p_{i,t}^{\mathrm{e}} - B_l^{\mathrm{w}} p_t^{\mathrm{wc}} + B_l^{\mathrm{d}} p_t^{\mathrm{ls}} \geq -\bar{\mathrm{f}}_l + B_l^{\mathrm{d}} D_t - B_l^{\mathrm{w}} \widehat{W}_t - \sum_{i\in\mathcal{G}^{\mathrm{CCP}}} h_{l,i}^{\mathrm{gen}} p_{i,t}^{\mathrm{fix}} - \sum_{i\in\mathcal{G}^{\mathrm{coal}}} h_{l,i}^{\mathrm{gen}} p_{i,t}^{\mathrm{e}} : \quad \left(\lambda^{\mathrm{lb}}\right), \tag{49}$$

$$-\sum_{i\in\mathcal{G}^{\mathrm{CCP}}} h_{l,i}^{\mathrm{gen}} p_{i,t}^{\mathrm{var}} x_{i,t} - \sum_{i\in\mathcal{G}^{\mathrm{GT}}} h_{l,i}^{\mathrm{gen}} p_{i,t}^{\mathrm{e}} + B_l^{\mathrm{w}} p_t^{\mathrm{wc}} - B_l^{\mathrm{d}} p_t^{\mathrm{ls}} \geq -\bar{\mathrm{f}}_l - B_l^{\mathrm{d}} D_t + B_l^{\mathrm{w}} \widehat{W}_t + \sum_{i\in\mathcal{G}^{\mathrm{CCP}}} h_{l,i}^{\mathrm{gen}} p_{i,t}^{\mathrm{fix}} + \sum_{i\in\mathcal{G}^{\mathrm{coal}}} h_{l,i}^{\mathrm{gen}} p_{i,t}^{\mathrm{e}} : \quad \left(\lambda^{\mathrm{ub}}\right) \Bigg\}. \tag{50}$$

where the objective of the lower level, (34), is to minimize the variable production cost of GTs and the CCGT-CCP, at the same time, minimize penalties due to wind curtailment or load shedding. c_i^{fuel}, c^{wc}, and c^{ls} are the coefficients of the marginal production cost of generators and the penalties of wind curtailment and load shedding, respectively. Note that for the CCGT-CCP, its variable production cost is calculated based on the CCGT's load level x_{it}, not its net electric power output. (35) enforces system-wide power balance in each dispatch period. (36)-(37) bounds the power output from GTs between their minimum and maximum values, which are denoted by $\underline{P}_i$ and $\overline{P}_i$, respectively. (38)-(39) guarantees GTs' upward and downward ramp rates are within their ramping capabilities, which are noted by $\acute{R}_i$ and $\grave{R}_i$. (40)-(43) is a similar set of constraints as (36)-(37), except that it regards the load level of the CCGT x_{it}, not the electric power output. (44)-(46) is the same set of constraints as (11)-(12) written in the normalized form. (47)-(48) restrains the wind curtailment and load shedding within the available quantity. (49)-(50) ensures the power flow on each transmission line is within the line capacity. The power flow is modeled by the power transfer distribution factor (PTDF), which belongs to the sensitivity factor subgroup of the DC power flow model, according to [30]. $\mathcal{L}$ is the index set of all transmission lines. $h_{l,i}^{\mathrm{gen}}$, B_l^{w}, and B_l^{d} are the PTDFs for all generators, wind farms, and system loads. As both the wind power and system load are considered to be aggregated, their PTDF matrices are multiplied by their bus-wise capacity vector and degenerate to a single dimension.

In (35)-(50), the greek symbols in the round brackets denote the sets of dual variables that correspond to the constraints before them. As will be introduced in the next Section, the dual variables are used to dualize the lower-level problem and transform the bi-level recourse problem into an equivalent single-level optimization problem.

C. THE COLUMN & CONSTRAINT GENERATION DECOMPOSITION ALGORITHM

The ARO UC problem is a tri-level optimization problem that is hard be solved in its original form. Decompositions

are often employed to derive equivalent forms that give tractability. In [28], Zeng and Zhao proposed to solve ARO UC problems using the column & constraint generation (C&CG) decomposition algorithm. It is iterative and proved to be finitely convergent. The algorithm follows a similar spirit as the classic Benders' decomposition (as used in [29]). It decomposes the original problem into a master problem that consists of the first-stage problem and under-estimators of the second-stage problem, and a set of subproblems that amount to the original second-stage problem with all first-stage variables fixed. The algorithm differs from the classic Benders' decomposition in that the under-estimator is constructed using the primal form of the second-stage problem rather than the sub-differential. The algorithm's effectiveness can be inferred similarly to that of the classic column generation algorithm. The subproblems serve as the pricing problems and populate critical scenarios, which correspond to vertices of the uncertainty set. For each identified critical scenario, a copy of the second-stage problem is added to the master problem, i.e., the generated columns and constraints. At the same time, a new under-estimator is introduced by an inequality constraint on the epigraph of the new copy of the second-stage problem. Every iteration in the algorithm tightens the master problem, leading to a non-decreasing sequence of lower bounds on the original problem. The algorithm stops either when a small enough gap between the upper and lower bounds of the objective function is achieved or when the subproblem returns a visited critical scenario. The finite convergence builds upon the finiteness of critical scenarios. Intuitively, C&CG could be treated as a clever combination of Benders' decomposition and column generation methods.

Using C&CG on (13)-(16), the master problem (till the k-th iteration) writes as [28]:

$$\boldsymbol{MP}: \quad \min_{\boldsymbol{y},\eta,\boldsymbol{x}^1\ldots\boldsymbol{x}^k} \boldsymbol{c}^\top \boldsymbol{y} + \eta \tag{51}$$

$$\text{s.t. } \boldsymbol{A}\boldsymbol{y} \geq \boldsymbol{d}, \tag{52}$$

$$\eta \geq \boldsymbol{b}^\top \boldsymbol{x}^i, \quad 1 \leq i \leq k \tag{53}$$

$$\boldsymbol{E}\boldsymbol{y} + \boldsymbol{G}\boldsymbol{x}^i \geq \boldsymbol{h} - \boldsymbol{M}\boldsymbol{u}^{*,i}, \quad 1 \leq i \leq k. \tag{54}$$

$$\boldsymbol{y} \in \mathcal{S}_{\boldsymbol{y}}, \tag{55}$$

where $\boldsymbol{u}^{*,i}$ refers to the critical scenario returned by the i-th subproblem; $\boldsymbol{x}^i$ is the corresponding generated columns; η is the auxiliary scalar variable used to construct the inequality on the epigraph of the second-stage problem.

Notice that even with all first-stage variables fixed, the second-stage problem still has a bi-level optimization structure. The classic Karush-Kuhn-Tucker conditions or the strong-duality theory could be used to reformulate the bi-level problem into a single-level equivalent. In this paper, the strong-duality-based reformulation is adopted:

$$\boldsymbol{SP}: \ \mathcal{Q}(\boldsymbol{y}) = \max_{\boldsymbol{u},\boldsymbol{\pi}} \left(\boldsymbol{h} - \boldsymbol{E}\boldsymbol{y} - \boldsymbol{M}\boldsymbol{u}\right)^\top \boldsymbol{\pi} \tag{56}$$

$$\text{s.t. } \boldsymbol{G}^\top \boldsymbol{\pi} \leq \boldsymbol{b}, \tag{57}$$

$$\boldsymbol{u} \in \mathcal{U}, \quad \boldsymbol{\pi} \geq 0. \tag{58}$$

Algorithm 1 The C&CG Algorithm

Initialize: $LB \leftarrow -\infty$, $UB \leftarrow +\infty$, $k \leftarrow 0$, $\epsilon \leftarrow$ non-negativereal number
while $(1 - LB/UB) \geq \epsilon$ **do**
1. Solve **MP** to have the optimal solution $\left(\boldsymbol{y}^{*,k}, \eta^{*,k}\right)$
2. Update $LB = \boldsymbol{c}^\top \boldsymbol{y}^{*,k} + \eta^{*,k}$
3. Solve **SP** with $\boldsymbol{y} = \boldsymbol{y}^{*,k}$ to have the new critical scenario $\boldsymbol{u}^{*,k}$
4. Update $UB = \min\left\{UB, \boldsymbol{c}^\top \boldsymbol{y}^{*,k+1} + \mathcal{Q}(\boldsymbol{y}^{*,k+1})\right\}$
if $\boldsymbol{u}^{*,k}$ turns out to be a repeated critical scenario **then**
break
end if
5. Generate $\boldsymbol{x}^k$ and add a new set of (53) and (54) to **MP**
6. $k \leftarrow k + 1$
end while
return $(\boldsymbol{y}^*, \eta^*)$

Bilinear terms that appeared in (56) can be exactly linearized by using the Fortuny-Amat & McCarl's trick [31], which usually goes by the name of the *big-M* method. The algorithmic procedure of the C&CG is summarized in Algorithm. 1.

IV. CASE STUDY

In this Section, the specifications of the case study are described. Computer programs are implemented in the Julia programming language [32]. The JuMP package [33] is used for the mathematical optimization modeling and the PowerModels package [34] for the power flow formulation. The latest Gurobi 10.0 [35] solves all the mixed-integer programming instances. Computation is conducted on a desktop computer with an Intel Core i7-10700 @ 2.90 GHz CPU and 16 gigabytes of RAM.

The case study is based on a modified 39-bus New England power system originally published in [36] and is now maintained in the case files library of MATPOWER [37]. The single-line diagram of the system is provided in Figure 3. The transmission system is untouched. Generators are reordered and assigned different technologies. G1 to G5 are coal-fired plants; G6 and G7 are GTs; G8 is the CCGT-CCP; W1 and W2 are aggregated wind farms. All generators keep their original capacity except G8, which is replaced with the proposed CCGT-CCP model. Fuel costs of all fossil plants are assumed to be affine functions. The coefficients of the cost functions are also modified. The case file is available online in [38].

The system load profile and wind power profile are provided in Figure 4. Bus-wise loads share the system load in proportion to the solved power flow in the case file. As W1 and W2 are aggregated, they follow the same profile, and their power outputs are proportional to their capacities. The error bounds of the wind power forecast are set to be $\pm 10\%$. The default value of the uncertainty budget is set to be 6.

For the CCGT-CCP model, coefficients and constant terms of the affine functions are tabulated in Table 2. The unit

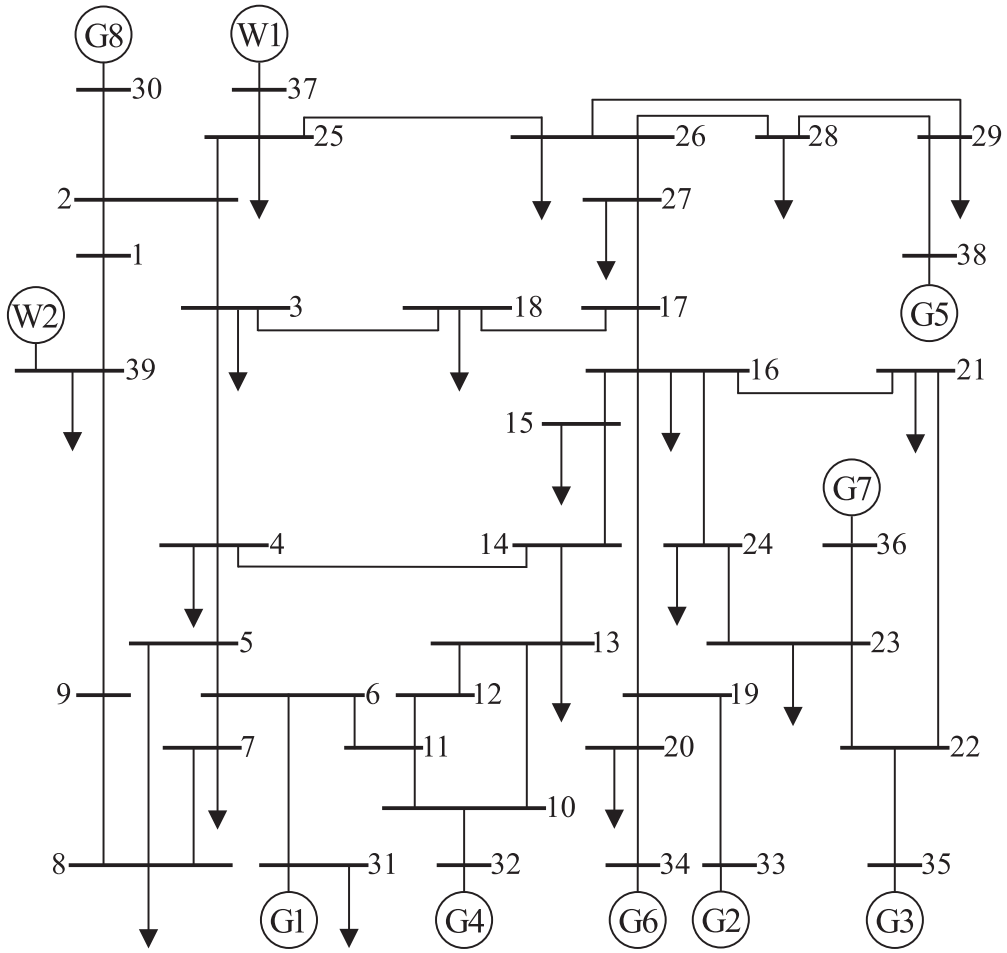

FIGURE 3. Single-line diagram of the modified 39-bus New England power system.

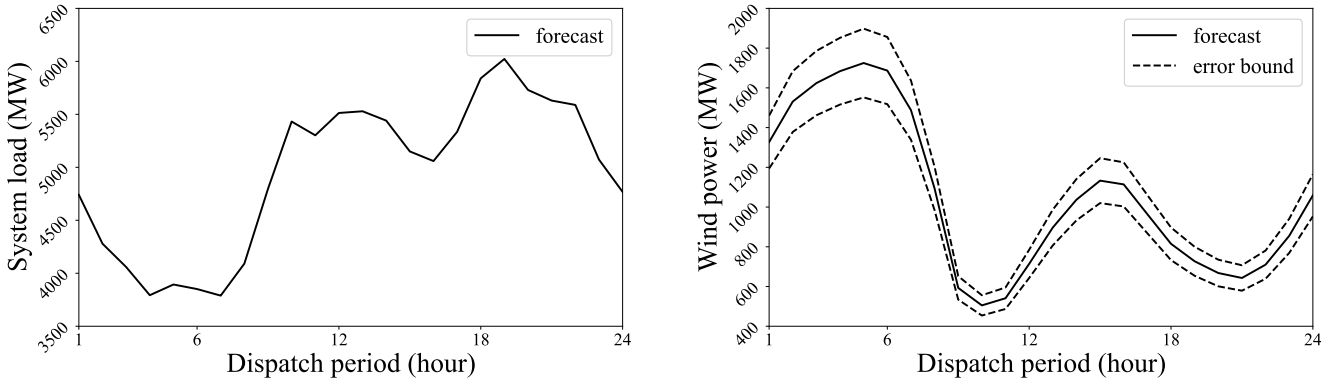

(a) System load forecast

(b) Wind power forecast and forecast error bounds

FIGURE 4. Forecast profiles for the case study.

of electric power is MW. The unit of solvent mass flow is kilogram/sec. The units of the first-order coefficients are denominated by percentage, respectively. The default value of solvent storage capacity is 6599×10^3 kilograms, equivalent to the solvent consumption under SS mode at maximum CCGT load for 1 hour. The initial stored solvent mass's default value is 80% of the solvent storage capacity.

TABLE 2. Coefficients in the CCGT-CCP model.

a_0^{rpl}	a_1^{rpl}	a_0^{ss}	a_1^{ss}	a_0^{mr}	a_1^{mr}	$a_0^{\text{sol,ss}}$	$a_1^{\text{sol,ss}}$	$a_0^{\text{sol,mr}}$	$a_1^{\text{sol,mr}}$
118.2278	6.9133	25.3040	0.5785	85.4385	−0.8305	457.3273	13.8051	1357.4277	−13.6226

TABLE 3. The ARO UC solution.

Unit No./ Op. mode	Dispatch period 1 - 24			
G1	1 1 1 1 1 1	1 1 1 1 1 1	1 1 1 1 1 1	1 1 1 1 1 1
G2	1 1 1 1 1 1	1 1 1 1 1 1	1 1 1 1 1 1	1 1 1 1 1 1
G3	1 1 1 1 1 1	1 1 1 1 1 1	1 1 1 1 1 1	1 1 1 1 1 1
G4	1 1 1 1 1 1	1 1 1 1 1 1	1 1 1 1 1 1	1 1 1 1 1 1
G5	1 1 1 1 1 1	1 1 1 1 1 1	1 1 1 1 1 1	1 1 1 1 1 1
G6	1 1 1 1 1 1	1 1 1 1 1 1	1 1 1 1 1 1	1 1 1 1 1 1
G7	0 0 0 0 0 0	0 1 1 1 1 1	1 1 1 1 1 1	1 1 1 1 1 1
G8	0 0 0 0 0 0	0 0 1 1 1 1	1 1 1 1 1 1	1 1 1 1 1 1
SS	0 0 0 0 0 0	0 0 0 **1** 0 **1**	0 0 0 0 0 0	0 **1** 0 0 0 0
MR	0 0 0 0 0 0	0 0 0 0 **1** 0	0 0 0 **1 1** 0	0 0 0 0 0 **1**

For Gurobi, the MIP gap is set to be 1e−6, and the integer tolerance is set to be 1e−8 for both the master problem and the subproblems. The convergence gap of the C&CG is set to be $\epsilon = 1\text{e}{-5}$.

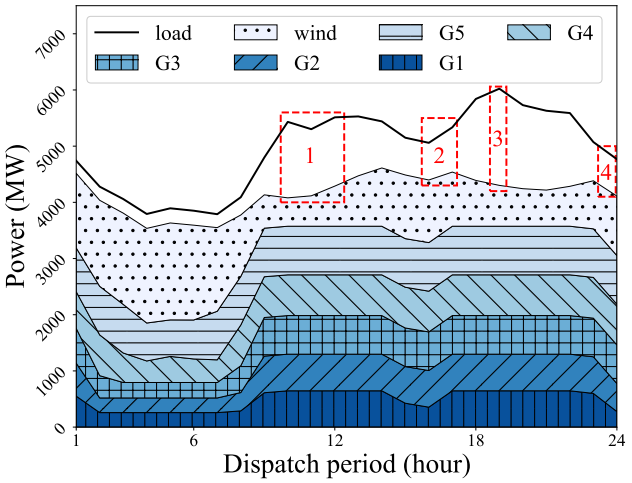

FIGURE 5. Power dispatch solution of coal-fired generators.

V. NUMERICAL RESULTS AND DISCUSSIONS

In this Section, numerical results are presented and discussed. Discussions are organized around four topics, each making up a subsection. Model parameters that are altered for analysis and comparison will be noted at the beginning of each subsection.

A. EFFECTIVENESS OF THE MODE-BASED CCP MODEL

UC solutions of G1-G8 under default values of the solvent storage parameters are tabulated in Table 3. As the system load is relatively heavy against the generation capacity, all coal-fired generators (G1-G5) and one GT (G6) must keep on in every period. Although CCGT-CCP (G8) has a slightly cheaper marginal cost than GTs, its minimum output power is larger than GTs. So, in the first 6-7 periods, G6 rather than G8 is committed. The last three rows in Table 3 indicate that constraints (5)-(7) are working properly. In each period, one mode at most is active. No mode activation happens when the host CCGT is off.

Besides, the pattern of the CCP operation mode transition matches the trend of the system load subtracting wind power and the coal-fired generators. In Table 3, there are four sets of mode transition sequences. First, a sequence of SS → MR → SS occurred during periods 10-12. Then, the MR mode is turned on for two consecutive periods. In period 20, the SS mode is activated. In the last period, the MR mode is again switched on.

The accordance between the transition sequence and the variation of the net load could be better shown in Figure 5. Notice the 'V' shape of the net load highlighted by the red dotted rectangle 1 in Figure 5. Remember that the power output of CCGT-CCP increases under the SS mode and decreases under the MR mode. The peak-valley-peak pattern resonates well with the first sequence. A surge of the net load happened in period 20, which is captured by rectangle 3. The surge coincides well with the activation of the SS mode in the same period. Don't forget that solvent circulation and storage also constrain the operation of the CCP. The CCP drains the storage under the SS mode, whereas it supplements the storage under the MR mode. In other words, the storage tank must have enough lean solvent before the SS mode could be called up. Such constraint explains why the MR mode is turned on during periods 16-17. Pinpointed by rectangle 2, it is clear that the net load drops to the lowest during these two periods before the surge in period 20. It is the best chance for the CCP to replenish the solvent at the lowest possible cost and prepare for the coming exhaustion in period 20. The last sequence could be interpreted following similar reasoning in conjunction with the daily solvent restoration constraint (12). After the exhaustion in period 20, the CCP seeks to restore the solvent level in the storage tank at the lowest cost. It can be seen in rectangle 4 that after period 20, the lowest net load appears in the final period.

To sum up, the simulation result validates the proposed mode-based model's effectiveness. They also confirm CCPs' positive contribution to the flexibility of the generation side.

B. ROBUSTNESS OF THE SOLUTION

To better understand the robustness of the solution given by the ARO framework, it is helpful first to look at the source of the robustness. Figure 6 depicts all 47 critical scenarios identified by the C&CG algorithm. Conceptually, the critical scenarios in ARO are similar to those in the stochastic programming framework. The recourse problem must be

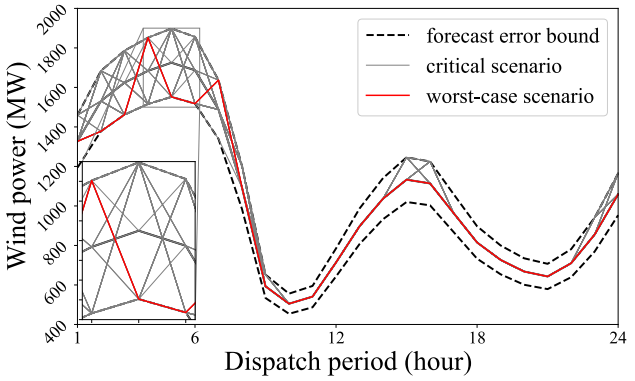

FIGURE 6. All critical scenarios of the wind power identified by the C&CG algorithm ($M = 6$).

feasible under every scenario simultaneously regarding the current first-stage solution. It is safe to say that the solution provided by the ARO framework is no worse than stochastic programming in the sense of its immunity to uncertainty.

The difference between the two frameworks resides in the conception of the scenarios. Scenarios in ARO result from the iterative pricing process in the C&CG algorithm, whereas the scenarios in stochastic programming are usually generated by Monte Carlo Simulation using the sample-average approximation. The former is *a posteriori*, while the latter is *a priori* to the optimal solution.

Note also that the availability of the critical scenarios in ARO is algorithm-dependent. If sub-differentials are used in the master problem instead of the primal form of the recourse problem, e.g., in the classic Benders decomposition, no specific scenario will be explicitly identified by the algorithm. The recourse problem is masked by its dual, less interpretable than the critical scenarios. Interpretability may count as one advantage of the C&CG algorithm over other alternatives.

However, further elaborations are needed when interpreting the robustness of the solution given by the ARO framework. One common pitfall, at least under the topic of power system operation planning, is to take the 'worst-case' scenario (the profile in red in Figure 6) as the 'dispatched' profile of the wind power. Such an understanding raises two issues.

- It mixes up the wind forecast from the actual wind power that is integrated into the grid. The former is solely determined by nature. Only the latter can be regarded as partially dispatchable since the utilized wind energy will never be greater than the available energy in the wind. Simply put, the integrated wind power equals the available wind power minus wind curtailment.
- It violates the rule of non-anticipativity. It can be checked that if the worst-case scenario is the only wind profile considered in the formulation, the optimal solution of the model will be less costly than the truly robust solution. The *expected value of perfect information* in stochastic programming (see Chapter 4.1 of [39]) also applies in ARO. In short, the robustness of the solution comes from the simultaneous consideration of multiple wind scenarios, not a single scenario.

As Section III-A mentions, the ARO focuses on finding the optimal value of the first-stage decisions, neither the second-stage decisions nor the uncertain variables. Only the first-stage decisions are concrete. The second-stage decisions are designed/considered hypothetical, against which quantitative assessments of the first-stage decisions are conducted. It does not decide what will be the actualization of the uncertainty.

The following test is designed to demonstrate the robustness of the optimal first-stage solution. One hundred wind power scenarios are randomly generated, assuming a uniform distribution on the interval between the error bounds, as shown in Figure 7. The optimal first-stage solutions under different uncertainty budgets (M) are substituted into the recourse problem to be tested against every generated wind power scenario. If the test problem is determined to be infeasible or the optimal value of the test problem is greater than the optimal value given by the ARO UC model, the test counts as a failure. Otherwise, it counts as a success. The failure rate is the number of failures divided by the total number of tests. The lower the failure rate, the higher the robustness of the first-stage solution.

The failure rates and statistics on other aspects of the test problems' optimal solutions are tabulated in Table 4 against the optimal solutions given by the ARO UC. The following three observations are ready to be made:

- The uncertainty budget reflects the decision-makers' risk-taking propensity. Risk-seeking propensity projects a lower uncertainty budget, while a higher uncertainty budget captures risk-averse. In this work, a lower uncertainty budget translates to a wind power profile that seldom deviates from the forecast. Consequently, the ARO UC model returns a lower estimate on the upper bound of the objective value of the recourse problem, which is shown in the 5th column in Table 4. This trend could be explained by the expensive GTs compensating for all wind power deviations. Higher estimates on wind power deviations invoke potentially more compensations from GT and, in turn, lead to higher operating costs.
- The uncertainty budget confines the robustness of the first-stage solution. In the 6th column, it can be seen that there is one failed test when $M = 4$. Notice also that its statistics on wind curtailments are the highest among the four data sets. The root cause lies in how the uncertainty budget shapes the optimal solution of the first-stage decisions. If the generation cost is to be minimized, coal-fired generators should produce as much energy as possible. However, higher dispatched from coal-fired generators leaves smaller re-dispatch room for GTs and the CCGT-CCP to compensate for the wind deviations. When the deviation of the truly realized wind power profile exceeds the estimates reflected by the uncertainty budget, wind curtailment is inevitable since little room for re-dispatch is left to flexible sources.

TABLE 4. Summary of the robustness test results.

M	ARO UC optimal solution				Test problem optimal solution								
	first-stage obj. values			recourse obj. values	failure rate	recourse obj. value				wind curtailment			load shedding
	start-up	fixed cost	coal fuel cost			max.	min.	avg.	std.	max.	min.	avg.	std.	
4	425.0	1879.3	8454.5	3964.1	1/100	3970.8	3659.0	3840.7	63.4	13.9	0.0	3.4	4.3	0.0
6	425.0	1879.3	8454.0	4028.5	0/100	3971.8	3660.0	3840.6	63.3	13.3	0.0	3.2	4.1	0.0
8	425.0	1879.3	8452.8	4082.1	0/100	3973.7	3661.9	3840.8	62.9	12.1	0.0	2.8	3.9	0.0
12	425.0	1879.3	8452.7	4172.6	0/100	3974.0	3662.9	3840.9	62.9	12.0	0.0	2.8	3.9	0.0

Notes: 1. The unit of the objective value is \$ 100; 2. the units of curtailed wind and shedded load are MW·h.

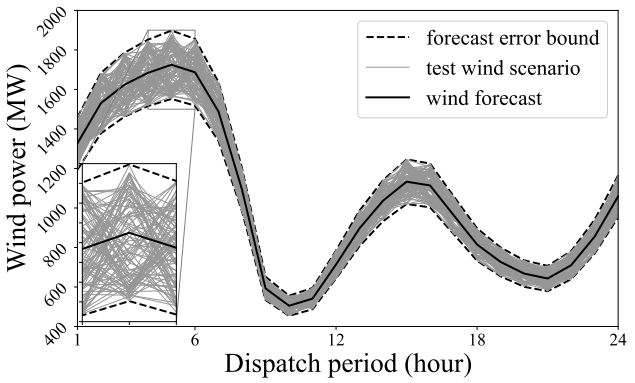

FIGURE 7. Generated wind power scenarios assuming uniform distribution.

The overall operation cost increases if the penalty due to the curtailed wind power overtakes the saved cost from dispatching more coal-fired power. This pattern can be sustained by the increasing trend of the fuel cost of the coal-fired generator in the first-stage solution (the 4th column) and the rising trend of statistics on wind curtailment (columns under the 'wind cur.' title) concerning lowered uncertainty budgets.

- The ARO framework is, in general, conservative towards uncertainty. Compared to the average optimal objective value of the test recourse problem, estimates given by the ARO UC model are uniformly higher. Even with a relatively low uncertainty budget, the estimate made by the ARO UC model is 1.03% higher than the test samples' average. Numerical results in Table 4 confirm such propensity towards conservatism, a consensus amongst the literature.

To sum up, the solution given by the ARO UC model is robust against the prescribed uncertainty. The uncertainty budget is vital to the solution's robustness.

C. SENSITIVITY ANALYSIS ON PARAMETERS RELATED TO SOLVENT STORAGE

Adding solvent storage into the solvent circulation loop grants improved operational flexibility to the CCPs. To some extent, the heat-intensive solvent regeneration process can then be temporally decoupled from the carbon absorption process. The storage tank's capacity limits the extent to which the decoupling achieves. A convenient measure of the storage

TABLE 5. Optimal ARO UC objective values under different $(\alpha, \overline{m})$ combinations.

Case No.	$(\alpha, \overline{m})$	total	coal fuel	recourse
1	$(0.2, 1)$	14787.5	8434.8	4048.4
2	$(0.5, 1)$	14785.9	8447.5	4034.1
3	$(0.8, 1)$	14786.8	8454.0	4028.5
4	$(0.2, 2)$	14786.1	8447.7	4034.1
5	$(0.5, 2)$	14780.8	8464.6	4011.8
6	$(0.8, 2)$	14783.3	8460.0	4019.0
7	$(0.2, 3)$	14784.5	8458.6	4021.5
8	$(0.5, 3)$	14780.8	8464.6	4011.8
9	$(0.8, 3)$	14780.8	8464.6	4011.8
10	$(0.2, 4)$	14784.5	8458.6	4021.5
11	$(0.2, 4)$	14780.8	8464.6	4011.8
12	$(0.2, 4)$	14780.8	8464.6	4011.8

Notes: The unit of the objective values is \$ 100.

TABLE 6. Dispatch results of case 1 v.s. case 10.

$\overline{m}$	GTs		CCGT-CCP	wind curtailment
	G6	G7	G8	
0.2	9017.0	4753.7	6558.6	0.0
0.8	9073.2	4559.9	6505.2	0.0

Note: the unit of the dispatch result is MW·h

tank's capacity is to count how many hours it can sustain when the CCP consumes or regenerates the solvent at the maximum rate. In the interest of determining its impact on the optimal objective values, the storage capacity measured in hours is altered to carry out a sensitivity analysis. The default value of the storage capacity is 1 hour. In [8], the storage capacity is 4 hours. Hence, setting the capacity from 1 hour to 4 hours seems sensible. A less obvious and almost neglected parameter regarding solvent storage is the initial solvent level in the storage m_0. The following definition is proposed to expose better the implication from the initial solvent level:

$$m_0 = \alpha \cdot \overline{m}, \quad \alpha \in [0, 1], \tag{59}$$

where α is called the *initial solvent ratio*. Let α take either 0.2, 0.5, or 0.8. The corresponding optimal solution of the ARO UC problems are tabulated in Table 5. As the first-stage commitment costs are identical under all settings, the corresponding cost terms are ignored in Table 5.

It can be seen that regardless of what the value α takes, larger storage capacity leads to a lower estimate of the recourse cost, a higher first-stage cost, and comprehensively

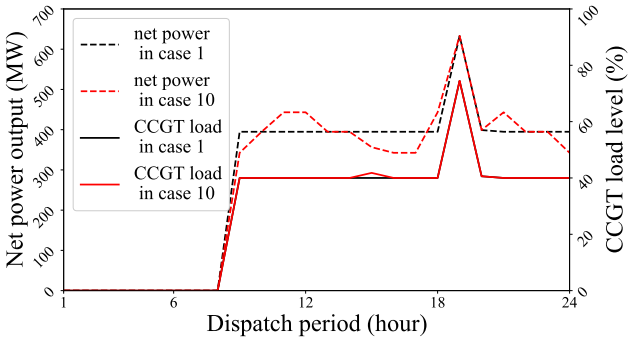

FIGURE 8. CCGT-CCP's load level and net power output in case 1 v.s. case 10.

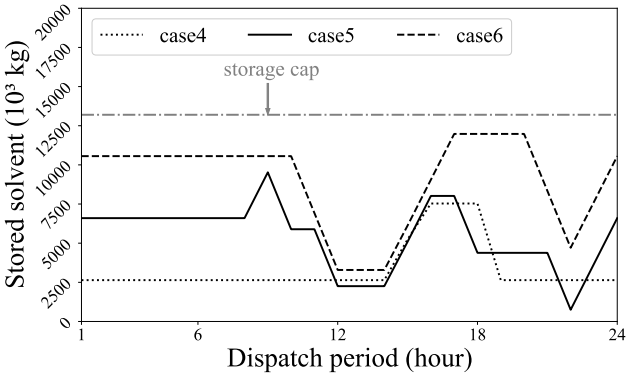

FIGURE 9. CCP's stored solvent in case 4, 5 and 6.

TABLE 7. Optimal objective values: mode-CCP v.s. lin-CCP.

CCP model	first-stage obj. values			recourse obj. values
	start-up	fixed cost	coal fuel cost	
mode-CCP	425.0	1879.3	8464.6	4011.8
lin-CCP	425.0	1879.3	8454.6	4008.0

Note:The unit of the objective value is $ 100.

a lower total cost. Increased coal power cost means coal-fired generators are dispatched to produce more energy. Following the analysis from the previous subsection, the re-dispatch room left to the flexible GTs and the CCGT-CCP is decreased. It is seemingly contrary to the also decreasing trend of the estimate on the recourse cost, which should be larger when the re-dispatch room is limited. The experiment below is conducted to unearth the root cause of this pattern.

The first-stage solutions of **case 1** and **10** are tested against the same wind power scenario using the recourse problem. The dispatch results are broken down to each generator and listed in Table 6 for comparison.

According to the results, no wind curtailment happens in both cases. So, the net load must also be the same under both cases because the load profile and the wind power scenario are exactly the same. The total dispatched energy in **case 1** is slightly lower than in **case 10** but still matches the trend in the previous analysis. Note that G7 has the highest fuel cost among the three generators. It can be seen that in **case 10**, production from G7 drops nearly 200 MW·h. Production from G6 has increased by 56.2 MW·h.

The behavior of G8 appears to be unexpected. As G8's fuel cost is also lower than G7's, its production should also increase. However, G8's electricity production drops over 50 MW·h. One explanation is that the proposed model treats the electric power output of the CCGT-CCP as a proxy of the CCGT's load level, see (1)-(4) in Section II-D. Therefore, it is the load level (x) rather than the electric power (p^e) that is priced in the recourse objective function (34). Given that the same load level maps to altered electric power outputs under different CCP operation modes, it is not impossible for the CCGT's load to increase while the net electricity production decreases.

Figure 8 portrays the CCGT-CCP's load level and electric power output over time under the two cases. Now it is clear that the speculation is correct. The load level profiles are overlapped except at around period 15. The CCGT-CCP is dispatched to a higher production level in **case 10** than in **case 1**, even though the difference is small. From electric power output profiles, CCP's positive contribution to flexibility is undeniable. The strictly proportionate relation between the load level and the electric power output in **case 1** indicates that no operation mode transition ever happened to the CCP. With almost the same load level profile, the electric power output in **case 10** is much more responsive than in **case 1**, thanks to proper mode transitions of the CCP. Specifically, the reached operating range is [342.5, 633.0] MW in **case 10** and [394.8, 633.0] MW in **case 1**. The former is 21.96% wider than the latter.

The above results confirm that larger capacities of solvent storage contribute positively to the flexibility of the CCP. Recall the results in Table 5. The value of the initial solvent ratio also delivers commensurate impacts on the objective values of the ARO UC problem. For example, **case 5** already achieves the lowest total cost in all 12 cases with $\overline{m} = 2$. In contrast, **case 9** achieves the lowest with $\overline{m} = 3$. Worse, none of the 4 cases under $\alpha = 0.2$ achieves the exact low cost. From a cost-performance perspective, the initial solvent ratio might be even more useful than the solvent storage capacity in short-term operations. The former needs no additional investments and can be adjusted in the short term, while the latter requires relatively significant follow-on investments and can not be changed conveniently. It is, therefore, worthwhile to understand how the initial solvent ratio shapes the optimal solution to the UC problem.

Similar experiments as above are carried out on **cases 4, 5** and **6** to isolate the influence from the initial solvent ratio,. This time, the variations of the stored solvent under all three cases are plotted in Figure 9. As **case 5** achieves the lowest operation cost, it is chosen as the baseline. Notice also the grey cap line indicating the solvent storage capacity. Compared to **case 5**, the other two cases suffer from a limited upward or downward 'ramping' room. Taking **case 6** as an example, at around period 10, the CCP should activate the MR mode. However, due to a higher initial solvent ratio, there is

TABLE 8. Dispatch results: mode-CCP v.s. lin-CCP.

CCP model	GTs		CCGT-CCP	
	G6	G7	G8	CCGT load
mode-CCP	9026.9	4559.9	6505.2	676.9
lin-CCP	9098.6	4555.4	6486.4	666.2

Notes: 1. the unit of the dispatch results for G6, G7 and G8 is MW·h. 2. the unit of the CCGT load result is percentage.

not enough room in the storage tank for the CCP to run under the MR at the current load level for one hour. So, the CCP has to wait until period 11 to turn on the SS mode for two consecutive periods. For **case 4**, the difficulty comes from an opposite direction.

The presence of the daily solvent restoration constraint (12) in the proposed model reinforces the initial solvent ratio's impact. Constraint (12) implies a complementary relationship between the SS and the MR mode. In other words, whenever the SS mode is activated, the MR mode will be activated in future periods and vice versa. With the restoration and the initial solvent ratio going hand in hand, the CCGT-CCP's bias towards either direction of ramping (in electric power output) is vaguely determined. It tends to do downward ramping when $\alpha \leq 0.5$, upward ramping when $\alpha \geq 0.5$, and stays neutral when $\alpha = 0.5$.

It is tempting to argue that letting the CCGT-CCP stay neutral is the best strategy. The results in Table 5 also seem to call for such an argument. However, the genuine determining factor should be the shape of the load profile the CCGT-CCP serves. This factor can be highly case-sensitive. How α should be appropriately set is beyond the scope of this work. Nevertheless, the significance of the initial solvent ratio to CCGT-CCPs in short-term power system operation problems is unmistakable.

D. THE MODE-BASED CCP MODEL V.S. THE LINEAR CCP MODEL

In order to quantify the difference between the proposed mode-based CCP model and Chen's linear CCP model, the linear CCP model in [9] is adapted to the CCGT model in this paper. The resulting CCGT-CCP model is then substituted in the ARO UC model. All parameters of the case problem are set to be the same as in **case 5**. For clarity, the mode-based CCP model and linear CCP models' results are denoted by *mode-CCP* and *lin-CCP*, respectively.

Table 7 tabulates the optimal objective values of the two models. The overall objective value is reduced by 0.09% when lin-CCP is used. The start-up and fixed operating costs are identical, indicating that the UC solutions are not affected by different modeling of the CCP. However, the fuel costs of the coal-fired units are 1000 dollars higher for mode-CCP than lin-CCP, in addition to a mild rise in the recourse objective values. Such trends suggest that lin-CCP exhibits higher flexibility than mode-CCP. Nevertheless, a closer look into the dispatch results tells another story.

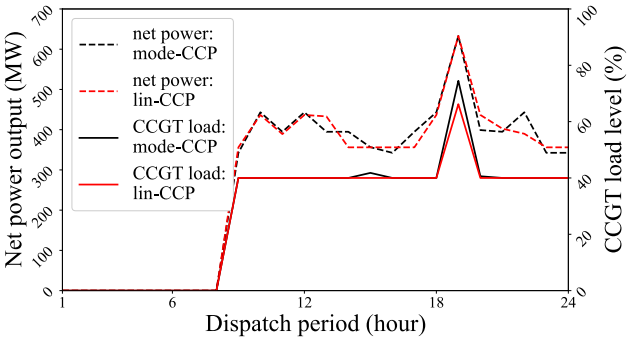

FIGURE 10. CCGT's load level and net power output: mode-CCP v.s. lin-CCP.

The CCGT's load level and net electric power output profiles of the two models are plotted in Figure 10. As shown by the dotted profiles, the operating range of lin-CCP (red) is narrower than mode-CCP (black). Specifically, the reached operating range of mode-CCP is between [342.5, 633.0] MW, 4.91% wider than lin-CCP's range of [356.1, 633.0] MW. Besides, by matching the CCGT's load level profiles to the net power profiles, it is clear that the energy penalty model of lin-CCP is different from mode-CCP. Take the dispatch period 19 as an example. Both models give the same net electric power output as mode-CCP while the CCGT load level given by lin-CCP is less than mode-CCP, which is 66.2% v.s. 74.5%. Note that the gap of 8.2 percentage points amounts to a difference of around 70 MW in gross power output. The above two observations indicate that lin-CCP underestimates the energy penalty from CCP compared to mode-CCP.

In Table 8, the dispatch results of fast-acting units are listed. Please be reminded that G6 has the lowest marginal production cost among the three units. When using lin-CCP, the dispatched production of G6 is 71.7 MW·h higher than mode-CCP, whereas the dispatched production of G7 and G8 drops. It explains the lower recourse objective value achieved by lin-CCP. However, the total dispatched production of the three units is 50.2 MW·h lower for lin-CCP than mode-CCP. It matches the $ 1000 reduction in coal-fired units' fuel cost.

To sum up, the overall optimal objective value of the ARO UC is slightly improved by 0.09% while the reached operating range of the CCGT-CCP is narrowed by 4.68% if the linear CCP model is adopted. Such changes are attributed to underestimated energy penalty from the CCP in the linear model than the mode-based model.

E. COMPUTATIONAL PERFORMANCE OF THE C&CG ALGORITHM

There are 15 cases in previous subsections where the full ARO UC model is solved using the C&CG algorithm. Algorithmic parameters are kept the same, as stated in Section IV. As the scale of the benchmark system is moderately large, and various combinations of physical model parameters have been tested, the cases may count as empirical evidence of the computational performance of the C&CG algorithm for

TABLE 9. Statistics on the computational performance of the C&CG algorithm.

ϵ	final optimality gap				critical scenarios count				computation time (s)			
	max.	min.	avg.	std.	max.	min.	avg.	std.	max.	min.	avg.	std.
1.0e−5	7.9e−14	2.0e−14	4.7e−14	2.2e−14	51	25	41	7	1510.4	200.9	714.5	462.3

real-world applications. Statistics on the results from the 15 cases are tabulated in Table 9.

As the statistics on the optimality gap of the last iteration suggest, the exact optimal solution of the ARO UC problem is found in all 15 cases. The optimality gap is defined as the relative difference between the upper bound and the lower bound of the optimal objective value. The data could be attributed to the rounding errors due to finite-precision arithmetics of float numbers. Interestingly, the value chosen for the convergence gap ϵ works exceptionally well.

The count on the identified critical scenarios is one order of magnitude larger than those in [40]. The mathematical structure of the proposed UC model may explain the drastic difference. In common UC models, only the commitment decision requires binary variables, which will also appear directly in the objective function. The UC model developed in this work introduces extra binary variables to indicate the operation modes of the CCP, which are not directly included in the objective function. The operation modes will change the level of flexibility of the CCGT and, in turn, change the optimality of the dispatch result. As the chain of cause and effect for the operation modes is longer than the commitment decisions, this may pose difficulties for the algorithm. Besides, commitment decisions generally have higher sensitivities on the objective value than the operation modes indicators. Binary variables with lower sensitivities may cause troubles to the branch and bound algorithm in the MIP solver. The proposed model is computationally more challenging than common ARO UC formulations.

Computation time varies quite widely from case to case. The number of all identified scenarios also faces a similar situation. Indeed, there is a positive correlation between the computation time and the number of critical scenarios considered in the model. Recall the structure of the master problem (51)-(55) in the C&CG algorithm. The scale of the master problem groves linearly regarding the number of identified critical scenarios. However, due to heuristics in the MIP solver and the evolving numerical characterization of each instance of the master problem, the computation time may not be strictly monotonically increasing over the scale of the master problem or, more specifically, the number of critical scenarios.

Take **case 1** as an example. The convergence trajectory and computation time of the master problems at each iteration are plotted in Figure 11. It is shown by the bars that the computation time of an expanding master problem is not increasing monotonically. Another prominent pattern in Figure 10 is the downward staircase shape of the convergence

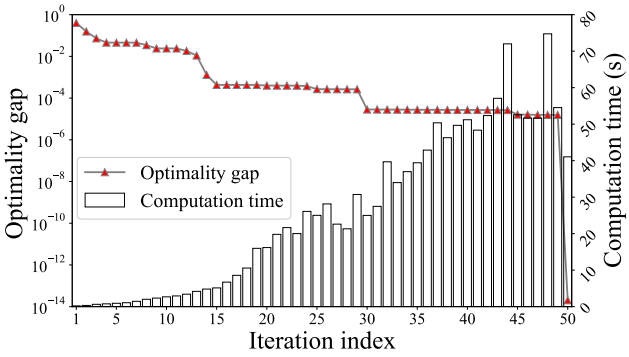

FIGURE 11. Convergence trajectory and computation time of case 1.

trajectory. The three apparent plateaus correspond to an order of magnitude of 10^{-2}, 10^{-4}, and 10^{-5}. At the end of the final plateau, the optimality gap falls off a cliff, indicating that the algorithm has found the true optimum. Combining the pattern with the accumulated computation time, one would agree that the value of the convergence gap seriously impacts on the algorithm's computation speed. For instance, if set $\epsilon = 1e{-}4$, the algorithm will stop at iteration 31. The overall computation time will be 331.5 seconds, only a quarter of the time for finding the true optimum. There is indeed always a trade-off between efficiency and accuracy. However, even the worst case 1501.4 seconds run is way more fulfilling to the efficiency demand of day-ahead problems. As a result, solving the proposed ARO UC model using C&CG has the potential to be implemented for real-world application.

VI. CONCLUSION

In this paper, the flexible operation of the carbon capture plants is abstracted to a generic mode-based model. A mixed-integer electric power output model of this low-carbon high-flexibility generation technology is proposed, building upon results from state-of-the-art research on process modeling of the combined-cycle gas turbine generators with post-combustion carbon capture. The new model is applied to a day-ahead adaptive robust unit commitment problem where wind power is considered the source of uncertainty.

The correctness of the proposed mode-based CCP operation model is demonstrated. Compared to the linear CCP model, the proposed mode-based model achieves a 4.91% wider operating range in the net electric power output, although the overall optimal objective value is slightly increased by 0.09%. The proposed model is more accurate than the linear model since the latter assumes a constant reboiler heat duty, which underestimates the energy penalty

of the CCP. The practicality of the proposed adaptive robust unit commitment model is also validated. Using the C&CG algorithm, most problem instances can be solved under 15 minutes. Finally, the initial solvent ratio is demonstrated to be non-trivial to the generation flexibility of generators with carbon capture plants. An optimal setting of the initial solvent ratio enlarges the operating range by 21.96%.

The applicability of the proposed model is beyond short-term scheduling problems for bulk power systems. It is interesting to consider the proposed CCP model in expansion planning problems for distribution systems with several types of renewable energy [41]. The proposed model may also be used to relieve transmission congestion issues, together with other flexibility sources such as distributed generations [42]. The authors plan to tackle these issues in future work.

REFERENCES

[1] H. Pörtner, *Climate Change 2022: Impacts, Adaptation and Vulnerability* (Summary for Policymakers). Cambridge, U.K.: Cambridge Univ. Press, 2022.

[2] K. Hansen, C. Breyer, and H. Lund, "Status and perspectives on 100% renewable energy systems," *Energy*, vol. 175, pp. 471–480, May 2019.

[3] C. T. M. Clack, "Evaluation of a proposal for reliable low-cost grid power with 100% wind, water, and solar," *Proc. Nat. Acad. Sci. USA*, vol. 114, no. 26, pp. 6722–6727, Jun. 2017.

[4] H. Abubakr, J. C. Vasquez, K. Mahmoud, M. M. F. Darwish, and J. M. Guerrero, "Comprehensive review on renewable energy sources in egypt—Current status, grid codes and future vision," *IEEE Access*, vol. 10, pp. 4081–4101, 2022.

[5] N. A. Sepulveda, J. D. Jenkins, F. J. de Sisternes, and R. K. Lester, "The role of firm low-carbon electricity resources in deep decarbonization of power generation," *Joule*, vol. 2, no. 11, pp. 2403–2420, Nov. 2018.

[6] J. Li, Y. Hou, P. Wang, and B. Yang, "A review of carbon capture and storage project investment and operational decision-making based on bibliometrics," *Energies*, vol. 12, no. 1, p. 23, Dec. 2018.

[7] W. Wei, F. Liu, J. Wang, L. Chen, S. Mei, and T. Yuan, "Robust environmental-economic dispatch incorporating wind power generation and carbon capture plants," *Appl. Energy*, vol. 183, pp. 674–684, Dec. 2016.

[8] X. Li, R. Zhang, L. Bai, G. Li, T. Jiang, and H. Chen, "Stochastic low-carbon scheduling with carbon capture power plants and coupon-based demand response," *Appl. Energy*, vol. 210, pp. 1219–1228, Jan. 2018.

[9] R. Zhang, T. Jiang, L. Bai, G. Li, H. Chen, X. Li, and F. Li, "Adjustable robust power dispatch with combined wind-storage system and carbon capture power plants under low-carbon economy," *Int. J. Electr. Power Energy Syst.*, vol. 113, pp. 772–781, Dec. 2019.

[10] R. Zhang, K. Yan, G. Li, T. Jiang, X. Li, and H. Chen, "Privacy-preserving decentralized power system economic dispatch considering carbon capture power plants and carbon emission trading scheme via over-relaxed ADMM," *Int. J. Electr. Power Energy Syst.*, vol. 121, Oct. 2020, Art. no. 106094.

[11] L. He, Z. Lu, J. Zhang, L. Geng, H. Zhao, and X. Li, "Low-carbon economic dispatch for electricity and natural gas systems considering carbon capture systems and power-to-gas," *Appl. Energy*, vol. 224, pp. 357–370, Aug. 2018.

[12] Y. Xiang, G. Wu, X. Shen, Y. Ma, J. Gou, W. Xu, and J. Liu, "Low-carbon economic dispatch of electricity-gas systems," *Energy*, vol. 226, Jul. 2021, Art. no. 120267.

[13] Y. Ma, H. Wang, F. Hong, J. Yang, Z. Chen, H. Cui, and J. Feng, "Modeling and optimization of combined heat and power with power-to-gas and carbon capture system in integrated energy system," *Energy*, vol. 236, Dec. 2021, Art. no. 121392.

[14] G. Zhang, W. Wang, Z. Chen, R. Li, and Y. Niu, "Modeling and optimal dispatch of a carbon-cycle integrated energy system for low-carbon and economic operation," *Energy*, vol. 240, Feb. 2022, Art. no. 122795.

[15] Z. Zhang, J. Du, K. Zhu, J. Guo, M. Li, and T. Xu, "Optimization scheduling of virtual power plant with carbon capture and waste incineration considering P2G coordination," *Energy Rep.*, vol. 8, pp. 7200–7218, Nov. 2022.

[16] L. Ju, Z. Yin, X. Lu, S. Yang, P. Li, R. Rao, and Z. Tan, "A tri-dimensional equilibrium-based stochastic optimal dispatching model for a novel virtual power plant incorporating carbon capture, power-to-gas and electric vehicle aggregator," *Appl. Energy*, vol. 324, Oct. 2022, Art. no. 119776.

[17] Y. Wang, S. Gao, W. Jia, T. Ding, Z. Zhou, and Z. Wang, "Data-driven distributionally robust economic dispatch for park integrated energy systems with coordination of carbon capture and storage devices and combined heat and power plants," *IET Renew. Power Gener.*, vol. 16, no. 12, pp. 2617–2629, Sep. 2022.

[18] D. Yang, Y. Xu, X. Liu, C. Jiang, F. Nie, and Z. Ran, "Economic-emission dispatch problem in integrated electricity and heat system considering multi-energy demand response and carbon capture technologies," *Energy*, vol. 253, Aug. 2022, Art. no. 124153.

[19] Q. Chen, C. Kang, and Q. Xia, "Modeling flexible operation mechanism of CO_2 capture power plant and its effects on power-system operation," *IEEE Trans. Energy Convers.*, vol. 25, no. 3, pp. 853–861, Sep. 2010.

[20] N. Abdul Manaf, A. Qadir, and A. Abbas, "Temporal multiscalar decision support framework for flexible operation of carbon capture plants targeting low-carbon management of power plant emissions," *Appl. Energy*, vol. 169, pp. 912–926, May 2016.

[21] X. Chen, X. Wu, and K. Y. Lee, "The mutual benefits of renewables and carbon capture: Achieved by an artificial intelligent scheduling strategy," *Energy Convers. Manage.*, vol. 233, Apr. 2021, Art. no. 113856.

[22] S. R. K, L. K. Panwar, B. K. Panigrahi, and R. Kumar, "Modeling of carbon capture technology attributes for unit commitment in emission-constrained environment," *IEEE Trans. Power Syst.*, vol. 32, no. 1, pp. 662–671, Jan. 2017.

[23] T. Spitz, A. G. Díaz, H. Chalmers, and M. Lucquiaud, "Operating flexibility of natural gas combined cycle power plant integrated with post-combustion capture," *Int. J. Greenhouse Gas Control*, vol. 88, pp. 92–108, Sep. 2019.

[24] Z. Ji, "Low-carbon power system dispatch incorporating carbon capture power plants," *IEEE Trans. Power Syst.*, vol. 28, no. 4, pp. 4615–4623, Nov. 2013.

[25] M. Lucquiaud, H. Chalmers, and J. Gibbins, "Potential for flexible operation of pulverised coal power plants with CO_2 capture," *Energy Mater.*, vol. 2, no. 3, pp. 175–180, Sep. 2007.

[26] P. Martens, E. Delarue, and W. D'haeseleer, "A mixed integer linear programming model for a pulverized coal plant with post-combustion carbon capture," *IEEE Trans. Power Syst.*, vol. 27, no. 2, pp. 741–751, May 2012.

[27] R. Zhou, H. Sun, X. Tang, W. Zhang, and H. Yu, "Low-carbon economic dispatch based on virtual power plant made up of carbon capture unit and wind power under double carbon constraint," *Proc. CSEE*, vol. 36, no. 6, p. 1675, 2018. [Online]. Available: http://www.pcsee.org/CN/abstract/article_30379.shtml

[28] B. Zeng and L. Zhao, "Solving two-stage robust optimization problems using a column-and-constraint generation method," *Oper. Res. Lett.*, vol. 41, no. 5, pp. 457–461, 2013.

[29] D. Bertsimas, E. Litvinov, X. A. Sun, J. Zhao, and T. Zheng, "Adaptive robust optimization for the security constrained unit commitment problem," *IEEE Trans. Power Syst.*, vol. 28, no. 1, pp. 52–63, Feb. 2013.

[30] B. Stott, J. Jardim, and O. Alsac, "DC power flow revisited," *IEEE Trans. Power Syst.*, vol. 24, no. 3, pp. 1290–1300, Aug. 2009.

[31] J. Fortuny-Amat and B. McCarl, "A representation and economic interpretation of a two-level programming problem," *J. Oper. Res. Soc.*, vol. 32, no. 9, pp. 783–792, Sep. 1981.

[32] J. Bezanson, A. Edelman, S. Karpinski, and V. B. Shah, "Julia: A fresh approach to numerical computing," *SIAM Rev.*, vol. 59, no. 1, pp. 65–98, 2017.

[33] I. Dunning, J. Huchette, and M. Lubin, "JuMP: A modeling language for mathematical optimization," *SIAM Rev.*, vol. 59, no. 2, pp. 295–320, 2017.

[34] C. Coffrin, R. Bent, K. Sundar, Y. Ng, and M. Lubin, "PowerModels. JL: An open-source framework for exploring power flow formulations," in *Proc. Power Syst. Comput. Conf. (PSCC)*, Jun. 2018, pp. 1–8.

[35] Gurobi Optimization, LLC. (2022). *Gurobi Optimizer Reference Manual*. [Online]. Available: https://www.gurobi.com

[36] T. Athay, R. Podmore, and S. Virmani, "A practical method for the direct analysis of transient stability," *IEEE Trans. Power App. Syst.*, vol. PAS-98, no. 2, pp. 573–584, Mar. 1979.
[37] R. D. Zimmerman, C. E. Murillo-Sánchez, and R. J. Thomas, "MATPOWER: Steady-state operations, planning, and analysis tools for power systems research and education," *IEEE Trans. Power Syst.*, vol. 26, no. 1, pp. 12–19, Feb. 2011.
[38] L. Wang. (2022). *Case File of the Modified 39-Bus New England Power System*. [Online]. Available: https://github.com/WangLuyu33/CCGT-CCP-case-file
[39] J. R. Birge and F. Louveaux, *Introduction to Stochastic Programming*. Cham, Switzerland: Springer, 2011.
[40] L. Zhao and B. Zeng, "Robust unit commitment problem with demand response and wind energy," in *Proc. IEEE Power Energy Soc. Gen. Meeting*, Jul. 2012, pp. 1–8.
[41] S. Zhou, Y. Han, P. Yang, K. Mahmoud, M. Lehtonen, M. M. F. Darwish, and A. S. Zalhaf, "An optimal network constraint-based joint expansion planning model for modern distribution networks with multi-types intermittent RERs," *Renew. Energy*, vol. 194, pp. 137–151, Jul. 2022.
[42] Prashant, M. Sarwar, A. S. Siddiqui, S. S. M. Ghoneim, K. Mahmoud, and M. M. F. Darwish, "Effective transmission congestion management via optimal DG capacity using hybrid swarm optimization for contemporary power system operations," *IEEE Access*, vol. 10, pp. 71091–71106, 2022.

LUYU WANG (Graduate Student Member, IEEE) received the B.S. degree in electrical engineering and automation from the Hefei University of Technology, Hefei, China, in 2013, and the M.S. degree in electrical engineering from Zhejiang University, Hangzhou, China, in 2016, where he is currently pursuing the Ph.D. degree in electrical engineering.

His research interest includes robust optimization methods for power system operation and planning under uncertainty.

BOYOU JIANG received the B.S. degree in electrical engineering from the Huazhong University of Science and Technology, Wuhan, China, in 2020. He is currently pursuing the Ph.D. degree in electrical engineering with Zhejiang University, Hangzhou, China.

He is a Visiting Ph.D. Student with Aalborg University, Denmark. His research interests include frequency-aware economic dispatch and power system reliability.

YUNHUI SHI received the B.S. and Ph.D. degrees in electrical engineering from Zhejiang University, Hangzhou, China, in 2016 and 2021, respectively.

He is currently with the Power Dispatch and Control Center, State Grid Zhejiang Electric Power Company Ltd., Hangzhou. His research interests include multistage robust optimization applied to the optimal operation of power systems and integrated energy systems.

ZHE CHEN received the B.S. and Ph.D. degrees in electrical engineering from Zhejiang University, Hangzhou, China, in 2016 and 2021, respectively.

From 2018 to 2019, he was a Visiting Ph.D. Student with the Department of Electrical and Computer Engineering, Southern Methodist University, Dallas, TX, USA. He is currently with the Electric Power Research Institute, State Grid Zhejiang Electric Power Company Ltd., Hangzhou. His research interests include power system operation and planning, renewable integration, and power system reliability.